Phase stability, elasticity, and theoretical strength of polonium from first principles

Dominik Legut,[1,2,*] Martin Friák,[1,3] and Mojmír Šob[4,1]
[1]*Institute of Physics of Materials, Academy of Sciences of the Czech Republic, v.v.i., Žižkova 22, CZ-616 62 Brno, Czech Republic*
[2]*Faculty of Chemistry, Brno University of Technology, Purkyňova 118, CZ-612 00 Brno, Czech Republic*
[3]*Institute of Condensed Matter Physics, Faculty of Science, Masaryk University, Kotlářská 2, CZ-611 37 Brno, Czech Republic*
[4]*Department of Chemistry, Faculty of Science, Masaryk University, Kotlářská 2, CZ-611 37 Brno, Czech Republic*
(Received 16 September 2009; revised manuscript received 9 March 2010; published 22 June 2010)

Employing full-potential linearized augmented plane-wave method, we investigate the stability of Po in its ground-state simple cubic structure (α-Po) with respect to the trigonal spiral structure exhibited by Se and Te and to the displacive phase transformations into either tetragonal or trigonal phases. The origin of the phase stability of α-Po is analyzed with the help of densities of states, electronic band structures, and total energies of competing higher-energy structures corresponding to selected stationary points of the total energy. The electronic structures and total energies are calculated both within the generalized gradient approximation and local-density approximation (LDA) to the exchange-correlation energy as well as with and without inclusion of the spin-orbit (SO) coupling. The total energies are displayed in contour plots as functions of selected structural parameters and atomic volume. It turns out that the LDA calculation with SO interaction incorporated provides best agreement with existing experimental data and that the simple cubic structure of α-Po is stabilized by relativistic effects of core electrons. High elastic anisotropy of α-Po is explained as a consequence of its simple cubic structure and is compared with elastic properties of other crystal structures. Finally, an uniaxial tensile test for loading along the [001] and [111] directions is simulated; the corresponding theoretical tensile strengths calculated within the LDA+SO approach amount to 4.2 GPa and 4.7 GPa, respectively, which are the lowest values predicted in an element so far. According to Pugh and Frantsevich criteria, α-Po is predicted to be ductile. Also a positive value of the Cauchy pressure confirms the metallic type of interatomic bonding.

DOI: 10.1103/PhysRevB.81.214118 PACS number(s): 71.15.Nc, 71.15.Rf, 71.70.Ej, 62.20.D-

I. INTRODUCTION

Polonium was discovered by Maria Skłodowska-Curie in 1898 and was named after her country of origin, Poland (Polonia). Crystalline Po is known to exist in two allotropes, the α-Po and β-Po. The former exhibits the simple cubic (sc) structure, as the only known element crystallizing in this structure under ambient conditions, with lattice parameter $a=3.345$ Å (Ref. 1). The latter phase, β-Po, has been experimentally found to crystallize in the rhombohedral (trigonal) structure with the lattice parameter $a_R=3.359$ Å, the rhombohedral angle of 98°13′, and the atomic volume of 36.6 Å^3 (Ref. 2). Both structures may be continuously linked together by a trigonal deformation, i.e. the trigonal structure of β-Po is obtained if a relatively small uniaxial distortion is applied along the [111] direction to the simple cubic α-Po (the rhombohedral angle of which is 90°). Both allotropes coexist in the temperature range of $18-54\pm1.5$ °C (see, e.g., Ref. 3).

Next to its unique simple cubic structure, polonium is radioactive and has the record high number of isotopes, namely, 36, which inevitably leads to the presence of the radioactive-decay products in the studied samples. Strong radioactivity of Po makes thus experimental investigations of its physical and chemical properties rather difficult. Most of the accessible experimental data of Po are summarized in the last edition of the Gmelin Handbook.[4] Regrettably, experimental information on many properties, e.g., on elastic behavior, is not available. However, in order to complete the existing experimental data with parameters which are difficult to obtain, the *ab initio* electronic-structure calculations based on fundamental quantum mechanics may be used to provide reliably many of the missing material characteristics.[5,6]

To the best of our knowledge, the very first theoretical study of sc Po was carried out by Lohr[7] employing the extended Hückel linear combination of atomic-orbital method. Later studies performed by us[8–13] as well as in other groups[14–17] used the all-electron methods. Many of these studies addressed the question of existence of unique simple cubic structure of polonium and tried to identify an interaction or a mechanism causing its stability. Lohr[7] speculated that such an stabilizing agent might be the spin-orbit (SO) interaction but his considerations were not supported by sufficient quantitative arguments. Some of the later studies[16,18] reported the SO interaction as the stabilizing agent, too, but our calculations[10–13] identified the mass-velocity and Darwin terms as the reason for stability of the sc structure. Further, we also predicted a high elastic anisotropy of sc Po.[10] The factor of elastic anisotropy[19] of α-Po is actually the record low among all the known solids. This extreme elastic anisotropy was found to be an intrinsic property of the sc structure. Theoretical calculations predict that, upon application of relatively low hydrostatic pressures (1–3 GPa), the sc structure becomes unstable and Po may transform into two rhombohedral (trigonal) structures.

In this paper, we examine in more detail the stability of the sc structure of α-Po with respect to the trigonal spiral structure exhibited by Se and Te as well as with respect to tetragonal and trigonal deformations, analyze its elastic anisotropy, simulate uniaxial tensile tests for a loading along the [001] and [111] directions, determine corresponding theoretical tensile strengths and discuss its ductility as well as the anisotropy of its Poisson ratio.

TABLE I. Computational parameters used in our WIEN2k calculations: #**k** is the number of **k** points in the whole Brillouin zone of sc polonium, $\#\mathbf{k}_{sc}^{IBZ}$, $\#\mathbf{k}_{tri}^{IBZ}$, and $\#\mathbf{k}_{tet}^{IBZ}$ represent the number of **k** points in the irreducible parts of the Brillouin zone of simple cubic, trigonal, and tetragonal phases, respectively. We also list the radius of the muffin-tin spheres R_{MT} (see the text for details), the cutoff energy parameter $R_{MT}K_{max}$, the maximum value of l of partial waves inside muffin-tin spheres, l_{max}, and the largest reciprocal vector in the charge Fourier expansion, G_{max}.

Parameter	#**k**	$\#\mathbf{k}_{sc}^{IBZ}$	$\#\mathbf{k}_{tri}^{IBZ}$	$\#\mathbf{k}_{tet}^{IBZ}$
Value	6000	165	570	475
Parameter	R_{MT} (a.u.)	$R_{MT}K_{max}$	l_{max}	G_{max}
Value	2.85(2.5)	9	10	13

The paper is organized as follows. After Sec. I, Sec. II briefly describes the method used in our theoretical calculations and the calculational parameters employed. Section III is devoted to displacive phase transformations and their accomplishment with the help of homogeneous tetragonal and trigonal deformations. The results obtained are discussed in three subsequent sections. Section IV presents structural and elastic characteristics, electronic structures as well as a detailed analysis of the structural stability of α-Po and β-Po and the other higher-energy phases, Section V is devoted to elastic anisotropy of the simple cubic Po, and Sec. VI to its theoretical tensile strength, Poisson ratio, and ductility. The last Sec. VII summarizes the main conclusions and closes the whole paper.

II. METHODOLOGY

The majority of the results were calculated with the help of the full-potential linearized augmented plane-wave (FLAPW) code WIEN2k.[20] The values of input parameters ensuring the convergence of total energies at the level of ± 6 μRy/atom are given in Table I. For all calculations with SO interaction included, the value of the parameter $E_{max}=4$ Ry was sufficient. For the exchange-correlation energy, both the local-density approximation (LDA) (Ref. 21) and generalized gradient approximation (GGA) (Ref. 22) have been used.

There are two radii of Po muffin-tin spheres listed in Table I. The lower value was used for structures along the trigonal transformation paths (see their description below) and for the energetic comparison of Te and Po in trigonal spiral structures when the atoms are located quite close to each other, the higher value was employed in all the other calculations.

III. DISPLACIVE PHASE TRANSFORMATIONS

The displacive phase transformations proceed by means of cooperative displacements of atoms from their lattice sites and alter the crystal symmetry without changing the atomic order or composition. Often they may be simulated by an appropriate homogeneous deformation.[23] They often connect some higher-symmetry structures where symmetry-dictated extrema of the total energy occur[23,24] and, together with the other energy minima, they can thus identify metastable phases.

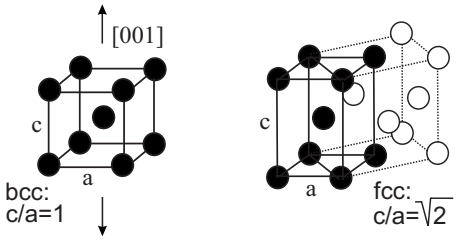

FIG. 1. The volume-conserving tetragonal (Bain) deformation path from the bcc to fcc structure.

Here we consider two simple transformation paths connecting cubic structures. They are the bcc-fcc transformation path via tetragonal deformation corresponding to extension along the [001] axis (the usual Bain path) and the trigonal deformation path that corresponds to uniaxial deformation along the [111] axis (Figs. 1 and 2). In the case of tetragonal deformation path, we start with the bcc structure considered as a tetragonal one with the ratio $c/a=1$, where c is measured along the [001] direction and a along a [100] direction. When c/a is varied, we arrive at body-centered tetragonal structures. There is one exception: for $c/a=\sqrt{2}$, the structure becomes fcc (Fig. 1). Similarly, we may consider the bcc structure as trigonal with the ratio of $c/a=1$, where c is measured along the [111] direction and a along a direction perpendicular to [111] (see, e.g., Ref. 23). If $c/a\neq 1$, the structure becomes trigonal except for $c/a=2$, when the sc structure is attained, and $c/a=4$, which corresponds to the fcc structure (see Fig. 2).

When studying the behavior of the total energy along the deformation paths, one usually assumes that the atomic volume is constant. Then both deformation paths discussed above may be fully parameterized by the ratio c/a. Its definition, however, is not unique. If the ground state of the studied cubic system is fcc, the path parameter for the tetragonal deformation path may be conveniently rescaled so that $(c/a)^{fcc}=1$ and $(c/a)^{bcc}=\sqrt{2}/2$. A similar rescaling of the trigonal path parameter (with $(c/a)^{fcc}=1$ and thus consequently $(c/a)^{sc}=1/2$ and $(c/a)^{bcc}=1/4$) was used in Ref. 14. Let us note that the above-mentioned cubic structures occur along these paths only in the case of pure elements. For intermetallics, the number of higher-symmetry structures is

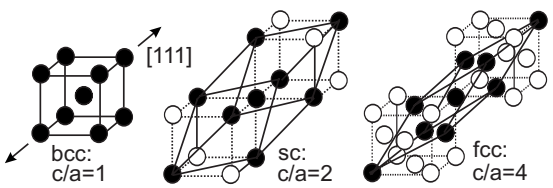

FIG. 2. High-symmetry structures obtained along the trigonal deformation path. The c and a are the lengths measured along the [111] direction and along a direction perpendicular to [111], respectively.

TABLE II. The equilibrium atomic volumes and bulk moduli of Po in various structures within the LDA and GGA. V_{exp} is the experimental atomic volume equal to 37.43 Å^3 (Ref. 1), V_{eq} are the calculated equilibrium atomic volumes. Values from the Ref. 16 correspond rather to LDA+SO calculations than GGA+SO (see the discussion in Ref. 13).

	V_{eq}/V_{exp}			
Struct./approx.	LDA	GGA	LDA+SO	GGA+SO
sc (FLAPW)	0.94	1.01	0.99	1.06
β-Po (FLAPW)	0.93	1.00	0.97	1.06
bcc (FLAPW)	0.82	0.88	0.87	0.95
fcc (FLAPW)	0.81	0.87	0.86	0.94
sc (FLAPW)[16]			0.99	
	Bulk moduli B (GPa)			
Struct./approx.	LDA	GGA	LDA+SO	GGA+SO
sc (FLAPW)	57.1	46.9	42.3	40.1
β-Po (FLAPW)	59.9	47.7	49.5	34.4
bcc (FLAPW)	65.5	55.0	50.3	34.8
fcc (FLAPW)	64.9	53.9	49.2	32.9
sc (FLAPW)[16]			44	

usually lower (see, e.g., Refs. 23 and 25). The structures occurring along the trigonal deformation path can also be described with the help of a rhombohedral unit cell with a single lattice parameter $a_R=b_R=c_R$ and the rhombohedral angle between diagonals of the unit-cell faces, α_R. The angle α_R for fcc, sc, and bcc structures equals to 60°, 90°, and 109°28′, respectively.

IV. RESULTS AND DISCUSSION

A. Structural and elastic characteristics

The total energy as a function of volume has been calculated for the simple cubic ground-state structure as well as for the rhombohedral β-Po, bcc, and fcc structures, without and with the SO interaction for the semicore 5d and valence 6s and 6p states. In the latter case (further denoted LDA+SO and GGA+SO, according to the approximation for the exchange-correlation employed), all relativistic effects for all electrons, i.e., mass-velocity and Darwin terms as well as SO interaction, are included. The former case (further denoted as LDA and GGA) comprises only the mass-velocity and Darwin terms for the semicore 5d and valence 6s and 6p electrons and is also referred to as scalar relativistic. Table II summarizes the theoretically determined equilibrium volumes V_{eq} and the bulk moduli B for these phases. In the case of the rhombohedral β-Po phase, the rhombohedral angle is kept fixed at its value corresponding to the equilibrium state of β-Po and only the volume is relaxed. It may be seen that only the GGA and LDA+SO calculations reproduce satisfactorily the experimental equilibrium volume. As the effect of SO coupling is strong in Po and must be incorporated, we consider the LDA+SO results as most reliable ones.

TABLE III. The structural energy differences (in mRy/atom) between various structures of Po without and with SO interaction (in parentheses) with respect to the total energy of simple cubic α-Po compared with the results of pseudopotential calculations (Ref. 14) and of another LAPW calculations (Ref. 15).

	LDA(+SO)	GGA(+SO)	LDA-PP (Ref. 14)	LDA (Ref. 15)
sc	0(0)	0(0)	0	0
β-Po	1.0 (0.7)	2.2 (1.9)		
bcc	14.5 (7.9)	18.5 (11.6)	16	8.5
fcc	20.1 (15.9)	24.6 (20.0)	22	13.5

As it can be seen from Table II, the calculations employing the LDA give the lowest equilibrium atomic volume of $V_{eq}^{LDA}/V_{exp}=0.94$. Quite similar underestimation within the LDA was found also in Ref. 15 ($V_{eq}/V_{exp}=0.93$ according to Fig. 7, $V_{eq}/V_{exp}=0.99$ according to Table 3) or when using the pseudopotentials[14] ($V_{eq}^{PP}/V_{exp}=0.94$). On the other hand, the equilibrium atomic volume calculated employing the GGA is slightly higher than the experimental one, $V_{eq}^{GGA}/V_{exp}=1.01$.

The inclusion of the SO interaction increases the equilibrium atomic volumes determined using both the LDA and GGA by about 4–7 % in all structures studied (see Table II). The equilibrium atomic volume of sc Po calculated within LDA+SO is $V_{eq}^{LDA+SO}/V_{exp}=0.99$, very close to the experimental value. The equilibrium volume within the GGA+SO is, on the other hand, considerably worse as compared to the previous GGA value, namely, $V_{eq}^{GGA+SO}/V_{exp}=1.06$.

Qualitatively similar increasing trend but quantitatively by a different value was also obtained when using the tight-binding approach[15] ($V_{eq}^{TB}/V_{exp}=0.925$, $V_{eq}^{TB+SO}/V_{exp}=0.95$, i.e., the increase of only about 2.5% in comparison with the case when the SO interaction is not included). In contrast to the second-order variation method used in WIEN2k code,[20] the inclusion of the SO interaction was not fully taken into account here but was included only *a posteriori* in the tight-binding calculations.

The expansion of the volume when the SO interaction is included is mainly caused by the behavior of the 6p states. The SO coupling lifts not only energetic degeneracy but both $6p_{1/2}$ and $6p_{3/2}$ states belong to different irreducible representations (Γ_6 and Γ_7,Γ_8) (Ref. 9) and therefore their spherical harmonics differ from each other.[26] Also, in this relativistic hybridization, the bonding to those states ($6p_{1/2}, 6p_{3/2}$) is restricted by geometry (volume) constraints.[27] As to bulk moduli, we observe a decreasing trend when comparing the results without and with the SO interaction. For example, in the case of the LDA and LDA+SO results, the inclusion of the SO interaction decreases the bulk modulus by about 25% in sc, bcc, and fcc Po.

Unfortunately, to the best of our knowledge, we are not aware of any experimental value of the bulk modulus of Po. In Table III of Ref. 15, the authors claim that the experimental bulk modulus of sc Po is 26 GPa, however they do not provide any reference and we were not able to find any ei-

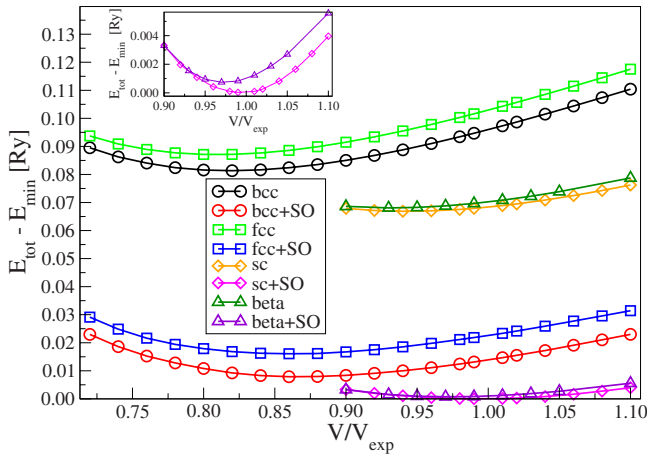

FIG. 3. (Color online) The LDA and LDA+SO energy-volume curves of Po calculated for the sc, β-Po, bcc, and fcc structures. The energy zero corresponds to the total energy of the equilibrium sc structure calculated within the LDA+SO. For a better clarity, the LDA results are rigidly shifted by 0.067 Ry/atom with respect to the LDA+SO results. The inset shows the behavior of total energies of sc and β-Po calculated within the LDA+SO in the neighborhood of energy minima.

ther. As all our FLAPW calculations as well as the calculations of other authors at the same volume concerning the bulk modulus of sc Po are in very good agreement, we believe that the bulk modulus of the α-Po would be considerably higher than 26 GPa.

B. Total-energy differences between various Po structures

In Fig. 3, we present the energy-volume curves of all structures considered with and without the SO interaction using the LDA. The total-energy order of individual structures as determined within the LDA(+SO) remains unaltered if GGA(+SO) is used instead (not shown).

The energy difference between the simple cubic α-Po and trigonal β-Po is very small (see the inset in Fig. 3). The values of the energy differences between various structures of Po with and without the SO interaction are summarized in Table III and compared with the results of other available calculations.

As it can be seen from Table III, when the SO interaction is included, the structural energy differences are decreased both within the LDA and GGA. Let us note that our calculated structural energy differences for bcc and fcc structures are very similar to those obtained in Ref. 14 and somewhat higher than those from Ref. 15.

C. Densities of states

The density of states (DOS) of the valence electrons characterizes the electron energy distribution for a particular structure. The comparison of DOS without and with SO coupling of the sc, β-Po, bcc, and fcc structures at their equilibrium volumes for LDA and GGA is displayed in Fig. 4.

We may see immediately that, in agreement with earlier studies, the $6s$ states are completely separated from the $6p$ states in all structures considered. This fact is known as the inert pair effect[28] which starts to occur in thallium (Xe $6s^2 6p^1$) and is also present in Pb and Bi. If the DOS of sc structure of Po is calculated without any relativistic corrections [see Fig. 4(a)], the nonrelativistic DOS exhibits very little separation between the $6s$ and $6p$ states (0.03 Ry) and therefore would allow much better mutual hybridization of these states if any instability occurs (e.g., Jahn-Teller distortion). Also, the widths of occupied $6s$ and $6p$ states (up to Fermi level) are nearly the same (approximately 0.43 Ry). If relativistic effects are included, we observe substantial contraction and a shift of the $6s$ states to lower energies [the upper edge of $6s$ band is shifted from about −0.45 Ry to about −0.80 Ry, Fig. 4(a)].

The lowest value of the DOS at the Fermi level belongs to the simple cubic structure, both without and with the SO interaction, indicating its relative stability with respect to the other structures (Table IV), and supporting the fact that the sc structure of Po is not stabilized by the SO interaction,[10] but, of course, this stabilization is enhanced when the SO interaction is included.[10,13]

Figure 5 shows the DOS of the $6p_{1/2}$ and $6p_{3/2}$ states in the sc structure. We may see that the pair of peaks at −0.37 and −0.32 Ry in Fig. 4(a) is predominantly due to $6p_{1/2}$ states.

Another interesting point regarding the DOS of bcc and fcc structures is a "pseudogap" located about 0.2 Ry above the Fermi energy [Figs. 4(c) and 4(d)]. If one looks at the bcc and fcc structures as the distorted sc structures occurring along the trigonal deformation path (bcc $\leftrightarrow$ sc $\leftrightarrow$ fcc, see Fig. 2) then the sc structure does not exhibit such a pseudogap in its valence $6p$ states. It is interesting to see that the inclusion of SO shifts the position of the pseudogap in the bcc and fcc structures by cca 0.09 Ry to higher values for both LDA and GGA.

D. Te-like trigonal structure of Po and Te

The close connections of the sc and trigonal (rhombohedral) structure was first realized by von Hippel.[29] He considered the trigonal structure of selenium and tellurium in hexagonal coordinates with lattice parameters a,c and with the internal parameter u. The sc structure is then obtained when the lattice parameters of the trigonal "Te-like" structure obey $c/a=\sqrt{3/2}\approx 1.225$ and the internal parameter equals $u=\frac{1}{3}$. Let us note that the experimental lattice parameters of Te are $a=4.451$ Å, $c=5.926$ Å, and $u=0.263$.[30]

To illustrate suppressing the Peierls distortion in sc Po, let us consider the DOS of Po in the trigonal Te-like structure. In Fig. 6, we plot different DOS where the internal parameter u as well as the c/a ratio were changed in constant volume calculations. We have calculated DOS for several positive and negative deviations of u as well as of the c/a parameter at the equilibrium volume obtained from the LDA (not shown) and LDA+SO (Fig. 6) calculations. The opening of the gap at the Fermi level (Peierls distortion) is clearly visible when the value of the c/a ratio is slightly shifted above the value of $c/a=\sqrt{3/2}$ corresponding to sc structure (see the upper part of Fig. 6, dotted curve). A more pronounced effect

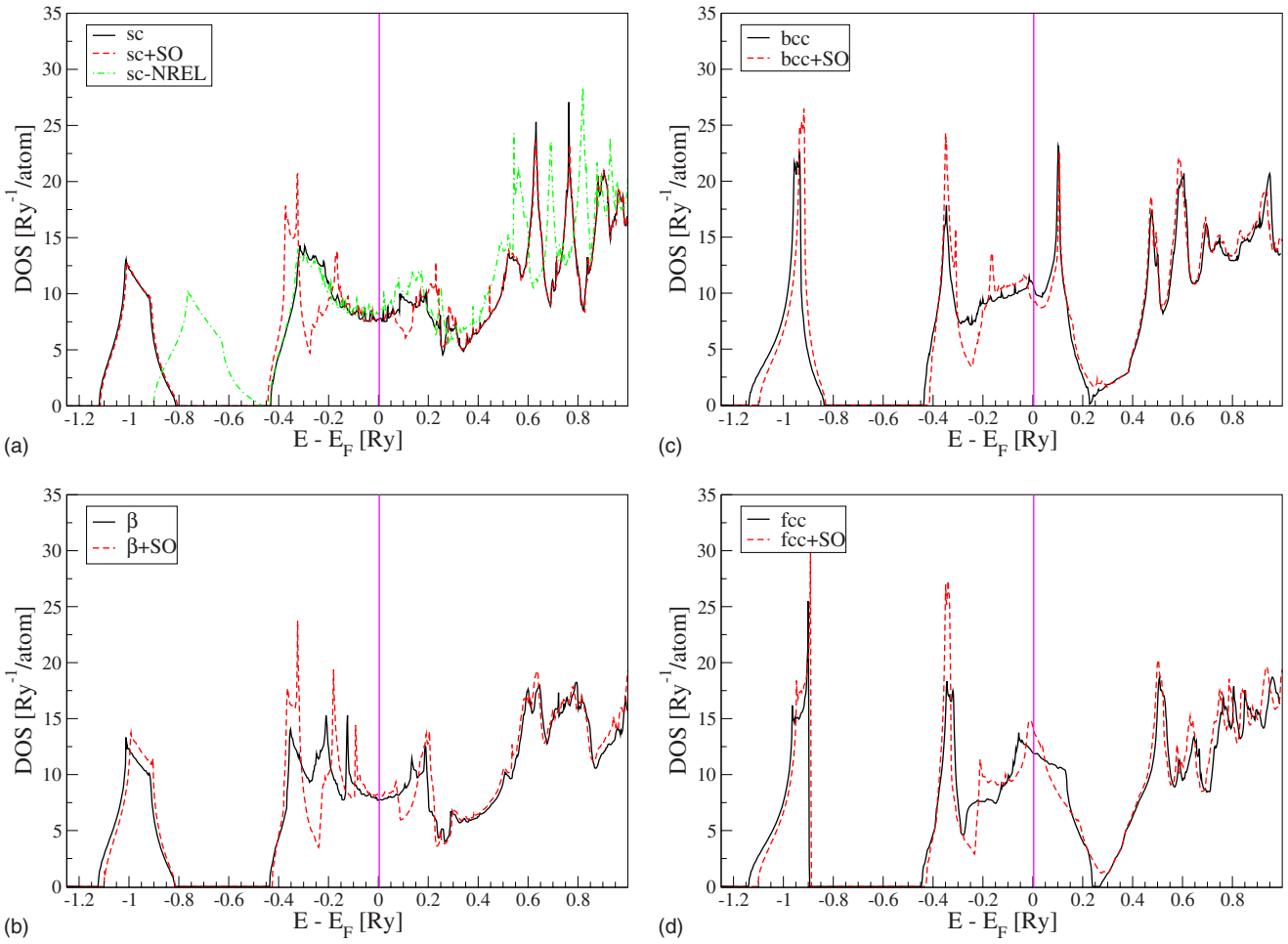

FIG. 4. (Color online) The density of states of Po in the sc, β-Po, bcc, and fcc structures at the corresponding equilibrium volumes with and without the SO coupling within the LDA.

on the opening of the gap and also on the shape of the DOS of the 6*s* states is observed when the internal parameter u is changed (see the lower part of Fig. 6, dotted and dashed curve).

Therefore, it is the suppression of the Peierls distortion that keeps Po in the sc structure in contrast to Te, where the Peierls distortion leads to two different nearest-neighbor distances and spiral trigonal chain structure. The energetics of both structures will be discussed in more detail in Sec. IV F.

E. Band structures

Here we would like to present and compare the band structures of Po in various structures with and without the inclusion of the SO coupling to see how the degeneracies of some energy states, found by group-theory analysis, develop. The dispersion relations (band structures) along high-

TABLE IV. The density of states (Ry^{-1}/atom) at the Fermi level DOS(E_F) of Po in the sc, β-Po, bcc, and fcc structural phases without and with the SO coupling calculated at the equilibrium atomic volumes.

DOS(E_F)	LDA	GGA	LDA+SO	GGA+SO
sc	7.68	8.40	7.66	8.96
β-Po	7.72	8.37	8.19	9.00
bcc	9.31	11.76	9.31	10.01
fcc	11.95	10.16	14.21	16.54

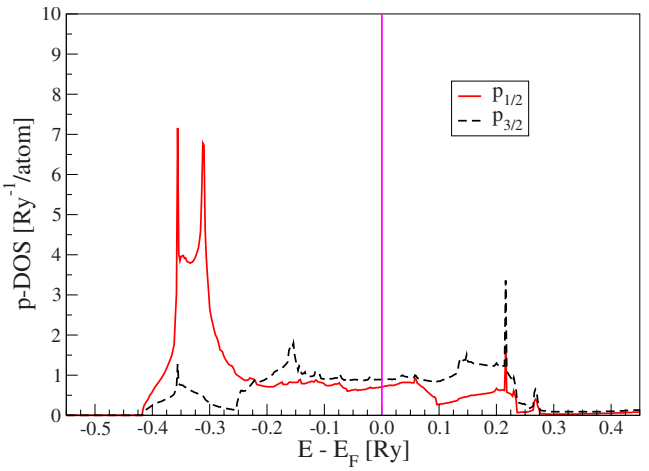

FIG. 5. (Color online) The projected DOS (per state) of twice degenerate $p_{1/2}$ and four times degenerate $p_{3/2}$ states in sc Po including the SO interaction within LDA. In contrast to Fig. 4, the DOS correspond to the RMT spheres (the interstitial contribution is omitted).

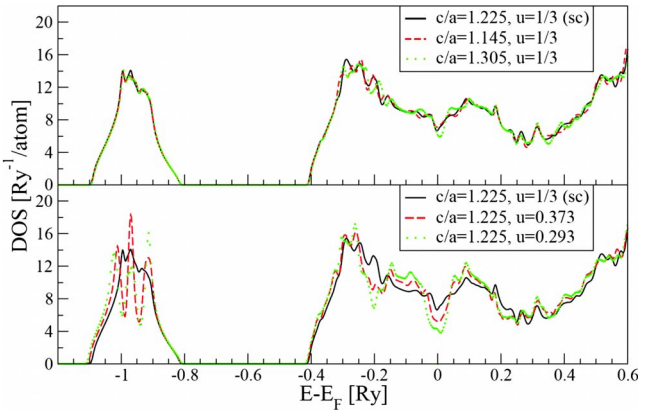

FIG. 6. (Color online) The DOS of Po in trigonal Te-like structure calculated within the LDA+SO where the onset of Peierls distortion is visible as c/a ratio (upper panel) or internal parameter u (lower panel) is shifted away from the sc structure.

symmetry directions in the first Brillouin zone for particular structures are shown in Figs. 7–13. The shapes of the band structures are very similar regardless of the exchange correlation used and the SO splittings of energy states at high-symmetry points are nearly identical. For comparison, we performed also nonrelativistic band-structure calculations (i.e., all core, semicore, and valence electrons were treated nonrelativistically—Fig. 7).

Comparing the nonrelativistic and scalar-relativistic band structure of sc Po (Figs. 7 and 8), we can see the almost identical shape and width of the valence occupied part of the p band. However, the width of the s band within the scalar-relativistic band structure is about 4 eV, considerably smaller

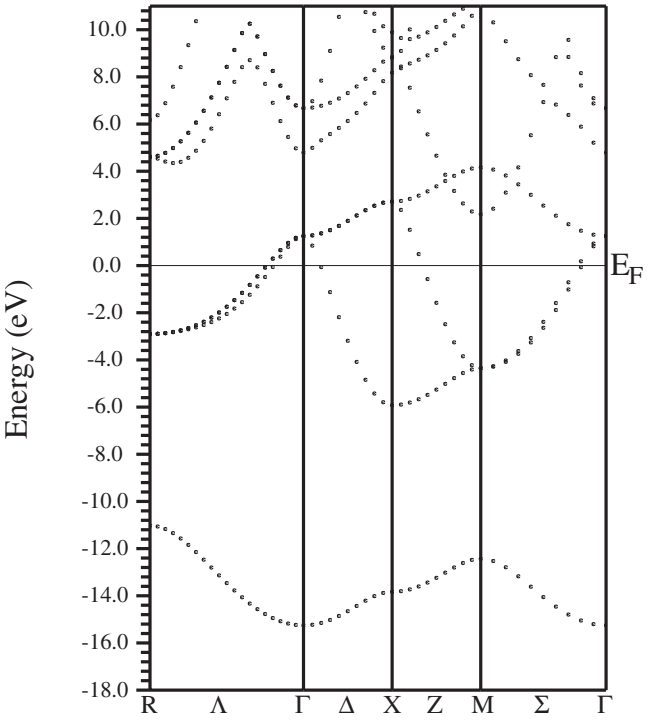

FIG. 8. The band structure of sc Po within the scalar-relativistic LDA calculation at the equilibrium atomic volume.

than in the case without any relativistic corrections when it amounts to cca 6 eV. Second, the separation between the s and p bands is higher in the scalar-relativistic case. Both trends are in accordance with the DOS already shown in previous section. When we include the SO coupling the split-

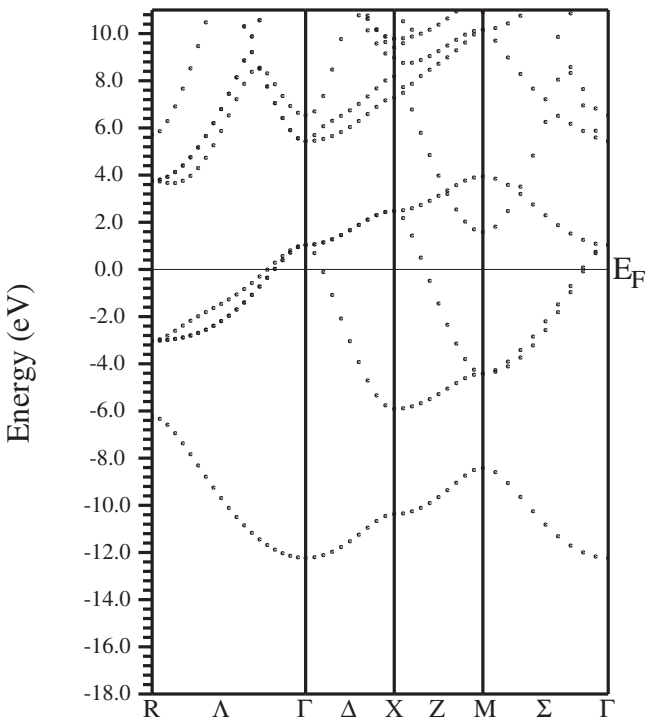

FIG. 7. The band structure of sc Po within the nonrelativistic LDA calculation at the equilibrium atomic volume.

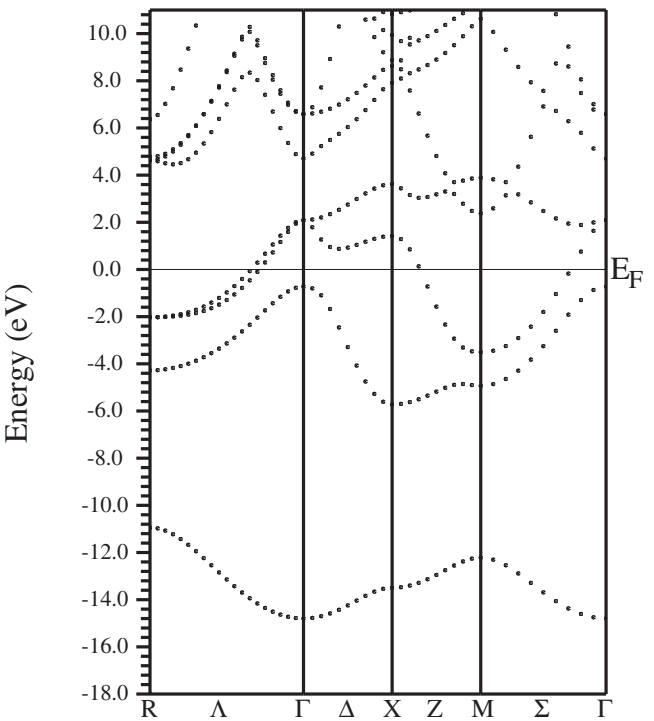

FIG. 9. The band structure of sc Po within the LDA+SO calculation at the equilibrium atomic volume.

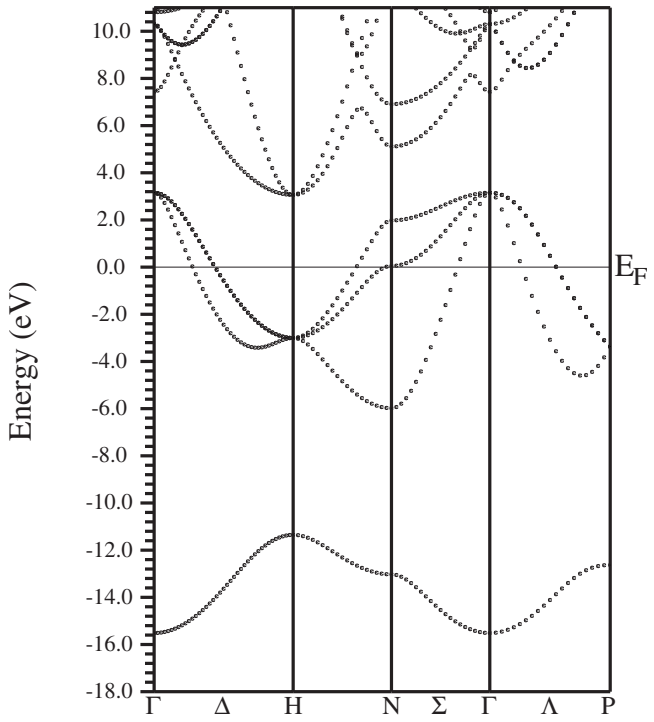

FIG. 10. The band structure of bcc Po within the scalar-relativistic LDA calculation at the equilibrium atomic volume.

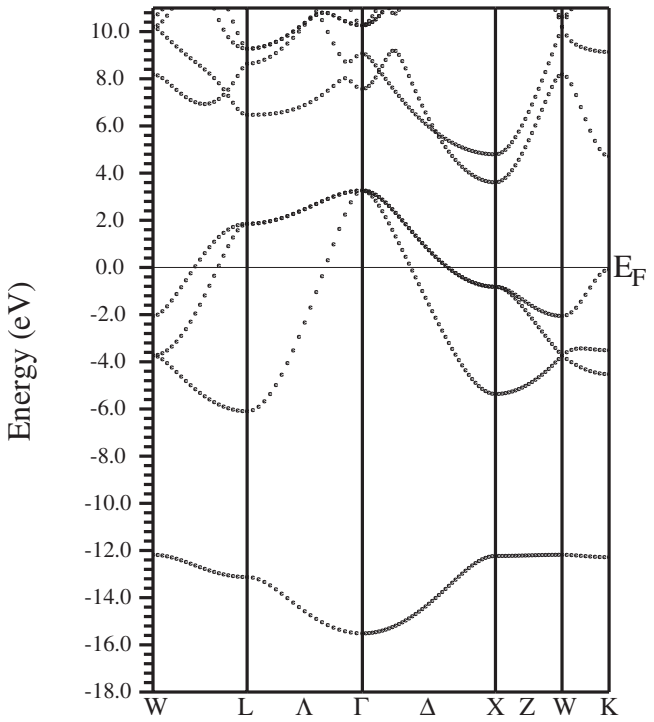

FIG. 12. The band structure of fcc Po within the scalar-relativistic LDA calculation at the equilibrium atomic volume.

tings of the *p* band occur (Fig. 9). The shapes of band structure with and without SO coupling calculated by the relativistically parametrized extended Hückel (REX) method in Ref. 7 are in very good agreement with our results, however, the SO splittings at high-symmetry points as well as the positions of the *s* and *p* band with respect to Fermi energy differ. This is rather understandable for a calculation done with the help of the extended Hückel approach. At the Γ point, the SO splitting of *p* band is about 2.7 eV (≈0.20 Ry), in a very good accordance with the value of

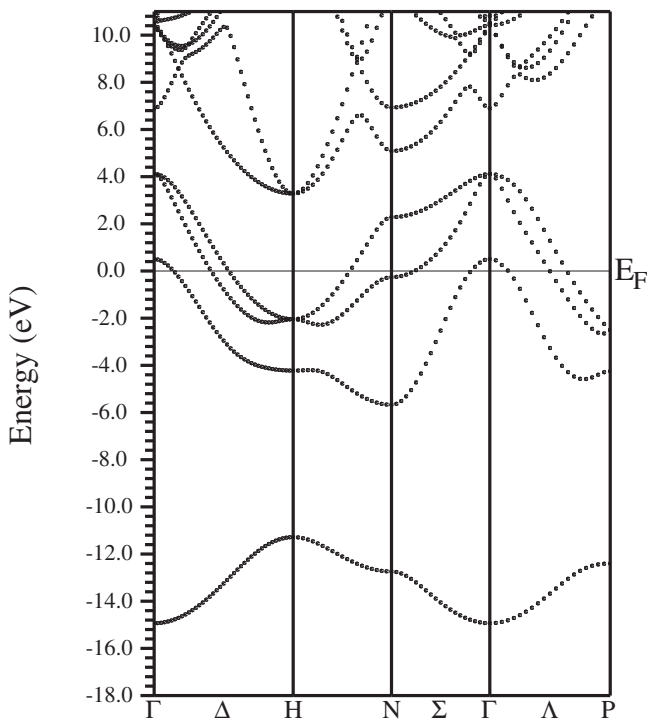

FIG. 11. The band structure of bcc Po within the LDA+SO calculation at the equilibrium atomic volume.

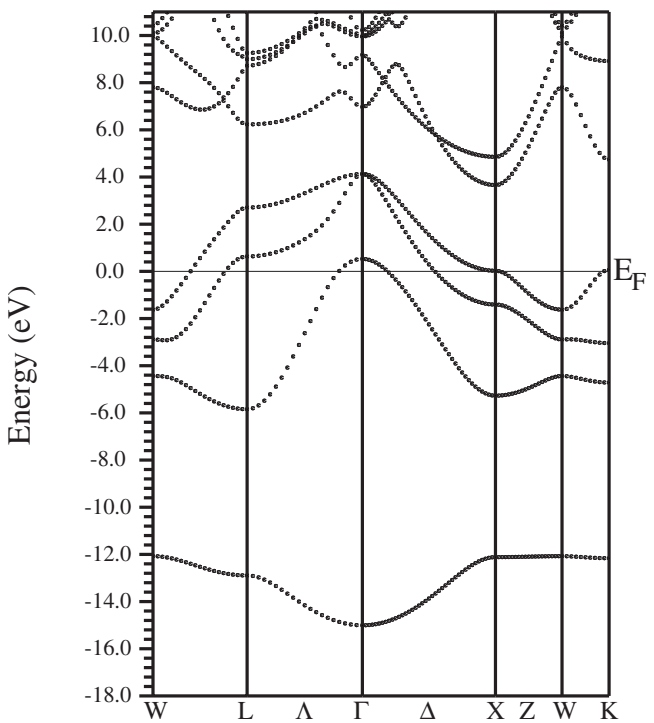

FIG. 13. The band structure of fcc Po within the LDA+SO calculation at the equilibrium atomic volume.

spin-orbit coupling constant ξ of Po atom. The splitting of the p band at R, X, and M points amounts to 2.3 eV, 2.2 eV, and 1.5 eV, respectively (Fig. 9). Earlier band-structure calculations of sc Po without SO interaction (Refs. 14 and 15) agree quite well with our dispersion relations.

Let us note that the sc structure is, among the other cubic structures studied, the only one that exhibits a crossing of two parabolic bands in the neighborhood of the point M at the energy of about 2 eV above the Fermi level (see Figs. 7–9). This may be connected with the existence of the pseudogap in the DOS of bcc and fcc Po and its absence in the DOS of sc Po, as shown in Fig. 4. The region of overlap of these two bands is somewhat reduced when the SO interaction is included.

Let us close this section by discussing the band structure of bcc and fcc Po with and without the SO coupling (Figs. 10–13). Below and in the neighborhood of the Fermi level, there is no band crossing at any **k** point with or without the SO coupling in contrast to sc Po. There is another striking difference in comparison with the sc Po with the SO coupling included. The bcc and fcc phases of Po have the upper edge of the lowest p band at the Γ point slightly above the Fermi level (0.2 eV, Figs. 11 and 13) but in the sc α-Po with SO coupling included the upper edge of this band is about 0.8 eV below the Fermi energy (Fig. 9). Also the absolute value of the SO splitting at the Γ point in the bcc and fcc Po is larger (3.5 eV) than in the sc α-Po (2.7 eV).

F. Stability of sc structure of Po

The simple cubic structure of Po is unique among the structures of elements in the periodic table. Also it differs from the isoelectronic elements of the 16th group, Se and Te. Although Te under pressure transforms into several other structures, the sc structure in Te has never been observed experimentally.[31]

To understand why polonium does not exhibit a trigonal spiral structure as Se and Te, we are looking for a term in the total energy of polonium which reverses the order of the trigonal Te-like and the sc structures or, in other words, which suppresses the Peierls distortion. Could it be a spin-orbit interaction that stabilizes the simple cubic structure of Po? Let us note that, in the following discussion, we are comparing total energies of all structures considered at their corresponding equilibrium atomic volumes. The equilibrium atomic volumes of sc and trigonal structure of Po and Te are different if calculated nonrelativistically, scalar relativistically, and scalar relativistically with SO interaction included (see Table II). As a general frame for our calculations, let us employ the trigonal spiral structure, the ground-state structure of Te, described in more detail in Sec. IV D.

In the following calculations, we use a hexagonal unit cell as in Ref. 16 but, instead of 847 **k** points in the full Brillouin zone, we employ 4000 **k** points. The crucial results have been checked with 15000 **k** points in the full Brillouin zone. In case of Po, one can see from Fig. 14 that if all relativistic effects (i.e., mass-velocity term, the Darwin term, and the SO interaction) for core, semicore, and valence electrons are included, then the lowest total energy with respect to c/a and u

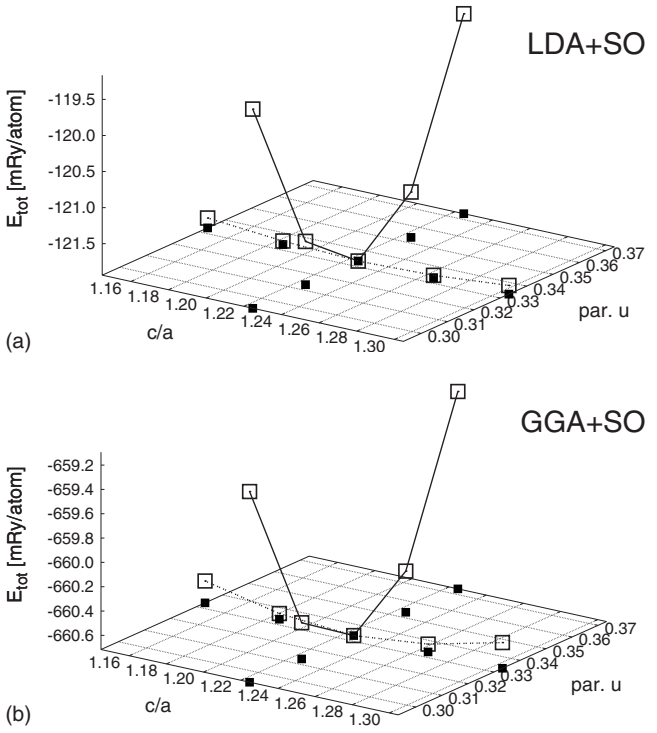

FIG. 14. The total energy of Po at the equilibrium atomic volumes (see Table II) as a function of c/a ratio and u parameter calculated within the LDA+SO and GGA+SO, i.e., with all relativistic effects included. The empty squares show the energies and the full squares positioned vertically under the empty squares mark the corresponding coordinates c/a and u. The full and dashed lines are guide for eyes only.

parameters is obtained for their values corresponding to the sc structure ($c/a=\sqrt{3/2}\approx 1.225$, $u=\frac{1}{3}$), both in the LDA+SO and GGA+SO calculations. In the case of Te, of course, if all relativistic effects are present, the ground-state trigonal spiral structure is preferred against the sc structure by 0.6 (2.4) mRy/atom using LDA (GGA) (see also Fig. 1 in Ref. 12).

Now, let us neglect the SO interaction but include the relativistic mass-velocity and Darwin terms for semicore 5d and valence 6s and 6p electrons (scalar-relativistic calculation). From Fig. 15, one can see that LDA calculation still favors the sc structure but in case of GGA, the results are not so convincing. Nevertheless, here we deal with very small energy differences and a small deviation from the ideal c/a ratio is within the calculational errors. Thus, we may conclude that within the scalar-relativistic LDA and most likely also within the scalar-relativistic GGA, the sc structure of Po is obtained as the ground-state structure and, therefore, it is not the SO interaction which stabilizes the sc structure of polonium. More details may be found in Ref. 10. Let us note that the recent pseudopotential LDA calculations of Verstraete[32] confirm this conclusion, i.e., that the scalar-relativistic terms are sufficient to stabilize the sc phase of α-Po. In the case of Te, if the SO interaction is omitted, the ground-state trigonal structure of Te is favored by 0.74 (2.8) mRy/atom with respect to sc structure using LDA (GGA) calculations.

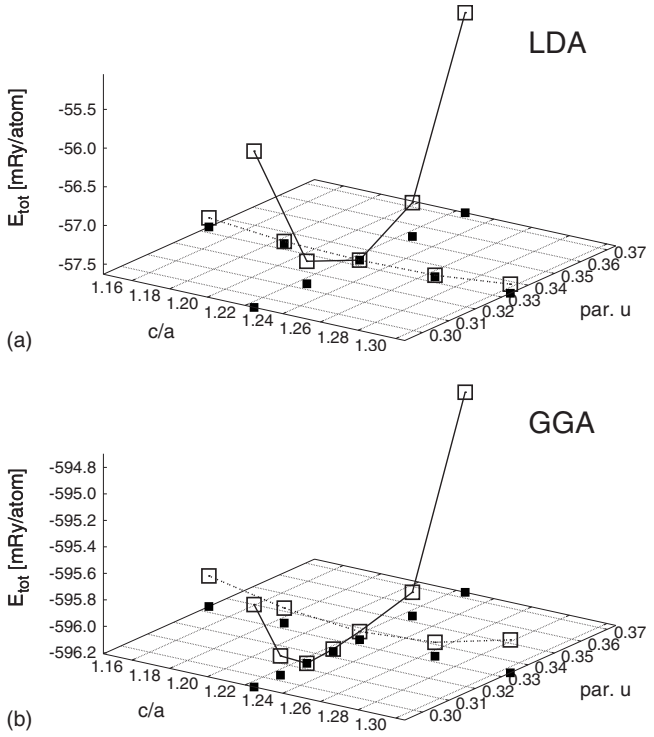

FIG. 15. The total energy of Po at the equilibrium atomic volumes (see Table II) as a function of c/a ratio and u parameter calculated scalar relativistically within the LDA and GGA, i.e., with the semicore and valence SO interaction neglected. The empty squares show the energies and the full squares positioned vertically under the empty squares mark the corresponding coordinates c/a and u. The full and dashed lines are guide for eyes only.

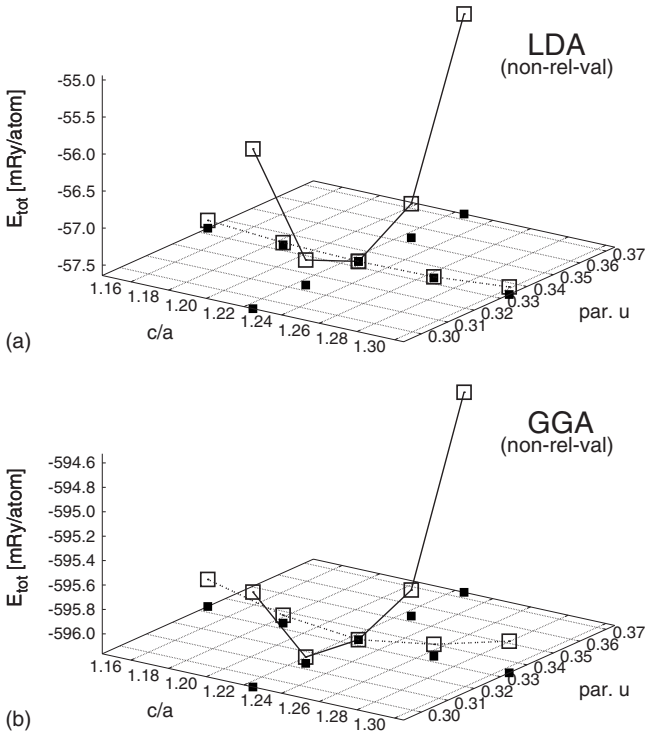

FIG. 16. The total energy of Po at the equilibrium atomic volumes as a function of c/a ratio and u parameter when the core states are treated relativistically but the semicore $5d$ states and valence $6s$ and $6p$ states are included nonrelativistically. The empty squares show the energies and the full squares positioned vertically under the empty squares mark the corresponding coordinates c/a and u. The full and dashed lines are guides for eyes only.

An interesting situation arises when we neglect all the relativistic effects for all states, including core states. (In most electronic structure codes, the core electrons are treated with the help of Dirac equation, therefore switching off the relativistic effects here means neglecting all of them, i.e., mass-velocity and Darwin term as well as the SO interaction.) Then, as we have shown in Fig. 2 in Ref. 10, Te still prefers the trigonal spiral structure by 1.9 mRy/atom using LDA but in case of Po, the situation is reversed: trigonal structure is favored with respect to sc structure by 0.3 mRy/atom. If we use GGA, we obtain very similar results: the total energies of trigonal spiral structures of Te and Po are lower than the energy of the sc structure by 3.9 mRy/atom and 0.3 mRy/atom, respectively.

To resolve which electrons indeed are responsible for this stabilization, we treated the semicore and valence-band states ($5d$, $6s$, and $6p$) nonrelativistically but included the core states relativistically. Such calculations lead to equilibrium atomic volumes which are very close to those of scalar-relativistic calculations. However, most importantly, the total energy of Po exhibits a minimum for $c/a=\sqrt{3/2}$, $u=\frac{1}{3}$, i.e., again for the sc structure, both in the LDA and GGA (Fig. 16). Therefore, we can conclude that the agent stabilizing the sc structure are relativistic effects of the core electrons—those lying under the $5d$, $6s$, and $6p$ shells. In a way, it is understandable—outer electrons are not subjected to the effect of heavy nucleus so much as the inner electrons. This illustrates a delicate interplay between various types of interactions determining finally the structure of α-Po and its properties. In this way, we may specify in more detail our conclusions given in Refs. 10 and 13 where we stated that it is the mass-velocity and Darwin term which stabilize the sc structure in Po. According to the present results, the decisive role in stabilization of the simple cubic structure in Po is played by the relativistic effects (i.e., the mass-velocity and Darwin term as well as the SO interaction) of the core states. It is these contributions to the energy that suppress the analogy of Peierls distortion and let Po be stable in its unique simple cubic structure.

This conclusion may be a little bit surprising. Namely, the Peierls distortion occurs due to the Fermi-surface instability, which is related to the Fermi-surface topology. In the case of polonium, however, the relativistic energy terms of core electrons influence the energetics of valence electrons and total energetics so much that if the relativistic effects for core electrons are switched off, even the ground-state crystal structure, determined primarily by valence electrons, is changed. Nothing like that is observed in tellurium, where relativistic effects (also for core electrons) are much weaker.

Here one could argue that a nonrelativistic calculation for core electrons is not meaningful, as the relativistic effects for core electrons cannot be neglected. However, omitting the SO interaction for semicore and valence electrons can be considered as equally questionable in such a heavy element

as Po (in this case, for example, the geometry of the Fermi surface is completely different when the SO interaction for semicore and valence electrons is switched off[16,32]). Therefore, the relativistic effects for the core electrons may be accepted as an agent stabilizing the sc structure in α-Po.

Naturally, we can always ask whether there can be any other stabilizing agent. As discussed in Ref. 13, we are looking for an effect which, when omitted, would change the sign in the energy difference between the Te-like structure and sc structure. Here we demonstrated that such an agent are relativistic effects for core electrons. The authors of Ref. 18 have found that SO interaction also leads to this effect but only if it is switched on or switched off solely for the 6*p* states. In this sense, both relativistic effects for core electrons and SO interaction for 6*p* electrons might be regarded as stabilizing the sc structure in Po.

G. Trigonal and tetragonal deformation path

In this section, we would like to explore the energetics along the trigonal and tetragonal deformation paths, especially with respect to bcc and fcc structures connected by these deformation modes, and look up how much is the total energy affected when we incorporate the SO coupling. As the ground-state structure of polonium is the sc structure, we should obtain the absolute minimum of total energy just for this structure along the trigonal deformation path at the equilibrium atomic volume. Concerning the tetragonal deformation path, we have chosen two different approaches. In the first one, we start from the ground-state sc Po and in the second one, we perform the tetragonal deformation from hypothetical structures of bcc and fcc Po similarly as for bcc W (Ref. 23) and fcc Pb (Ref. 33).

1. Trigonal deformation of sc Po

Let us discuss trigonal deformation path first. In most cases, the dependence of the total energy of Po on c/a ratio is rather simple, exhibiting the absolute minimum at the ground-state sc structure and a maximum at the other cubic structures. At those values of c/a, where the symmetry of the structure is higher than of those in the immediate neighborhood, the derivative of the energy with respect c/a must be zero.[24] As the GGA and LDA results are qualitatively very similar, we discuss only the LDA case here.

Figure 17 displays three curves. First, we may compare the total energy along the trigonal deformation path at equilibrium volumes with and without SO interaction. Second, the immediate effect of the change in the volume can be seen when a profile for a different volume (V_{exp}) is added. Also we changed the variable along the horizontal axis from c/a to $\ln c/a$ where the bcc, sc, and fcc structures are now at $\ln c/a=0$, 0.693, and 1.386, respectively. All energy profiles exhibit the absolute minimum for the ground-state sc structure. The curves rise at both sides of this minimum. At $\ln c/a=1.386$, we have found an extremum (maximum) dictated by symmetry for the fcc structure. The curves exhibit another symmetry-dictated maximum for the bcc structure at $\ln c/a=0$. It is understandable that these two maxima on the total-energy curve are accompanied by two outer minima: If

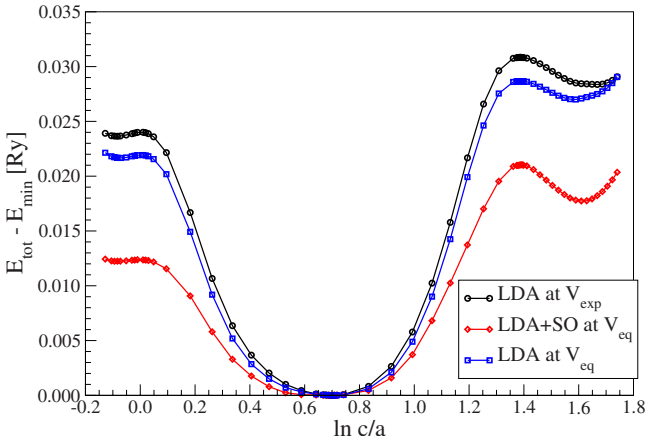

FIG. 17. (Color online) The total-energy profiles of Po at the equilibrium and experimental atomic volumes of the sc structure as a function of $\ln c/a$ along the trigonal deformation path obtained from the LDA calculations.

we decrease the c/a below 1 or increase above 4, atoms move very close to each other and the total energy increases due to the electrostatic repulsion. These minima, of course, are not dictated by symmetry. A minimum close to the bcc structure, when the $\ln c/a$ ratio becomes slightly negative, is very shallow. The other minimum behind the fcc structure ($\ln c/a > 1.386$) is considerably deeper. Similar features of the energy profile along the deformation path have already been reported in Refs. 8, 9, and 14. It may be seen from Fig. 17 that the inclusion of the SO interaction significantly decreases the total-energy differences between bcc and sc structure by 44% and between fcc and sc structure by 26% (cf. Table III, where the corresponding changes in energy differences at equilibrium volumes are 37–45 % and 19–21 %, respectively).

To see the behavior of total energy also at the other volumes, we have calculated the corresponding energy profiles at $V/V_{\mathrm{exp}}=0.80-1.05$ for LDA and LDA+SO and at $V/V_{\mathrm{exp}}=0.75-1.10$ for GGA (not shown) and GGA+SO. The total-energy profiles within the LDA+SO at several atomic volumes have already been reported in Fig. 1, Ref. 10. Here we show two-dimensional contour plots of total energy of polonium as a function of $\ln c/a$ and atomic volume (Figs. 18–20).

It may be seen that the ground state of sc Po corresponds to the absolute energy minimum, a bottom of the "basin" in the landscape of the total energy, marked by diamonds. Three auxiliary vertical lines denote the $\ln c/a$ ratio for bcc, sc, and fcc structures while the corresponding local maxima of total energy in one-dimensional plots (see Fig. 17 or Fig. 1 of Ref. 10) turn now into saddle points marked by triangles ($\nabla, \triangle$). As it was already pointed out those are the symmetry-dictated stationary points, they have to be there. However, very close to the bcc and not very far from the fcc stationary points, there are relatively shallow minima not dictated by symmetry; they are marked by heavy circles in Figs. 18–20. Their energy separation and distance from the bcc (fcc) structure for each contour plot are summarized in Table V.

These energy minima are best seen in total-energy landscape calculated within GGA with SO interaction included

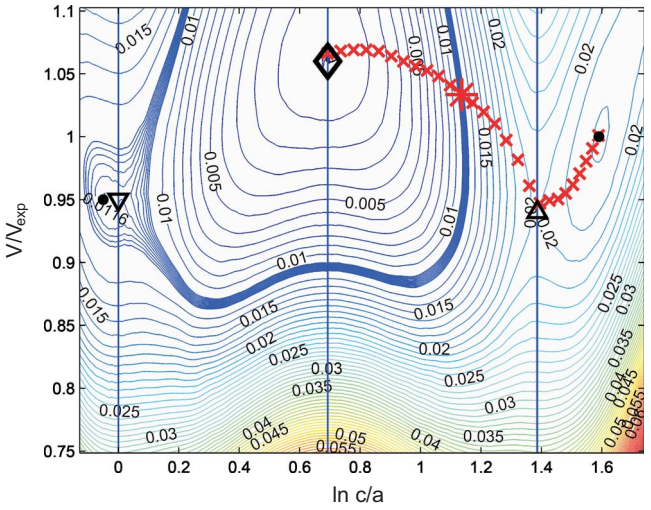

FIG. 18. (Color online) The contour plot of total energy of trigonally deformed Po calculated within the GGA with inclusion of the SO interaction. The sc structure is marked by a diamond (◇), the fcc by a triangle (△), bcc by an inverse triangle (▽), and the local minima close to bcc and fcc structures by full circles. For the purpose of identification of the stationary points, the energy contours are not equidistant. The crosses (×) correspond to the uniaxial tensile test along the [111] direction; a larger asterisk marks the inflection point indicating the configuration with the maximum tensile stress.

(Fig. 18). Here the bcc and fcc saddle points are accompanied by a local minimum from the outer side. The structure corresponding to the minimum close to the bcc structure has nearly the same atomic volume as the bcc structure at the

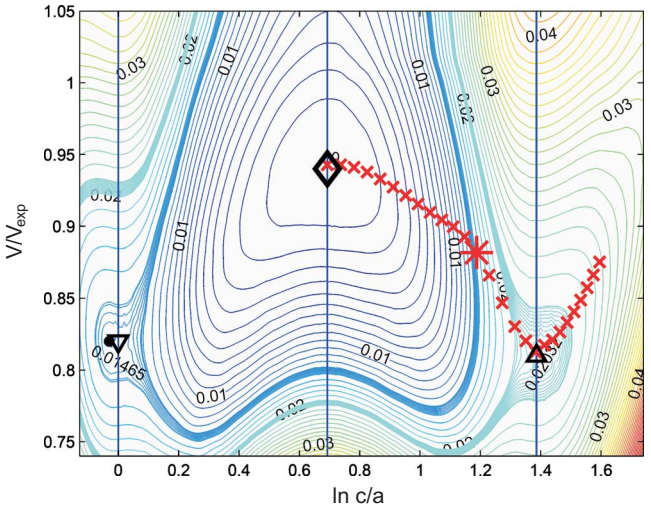

FIG. 19. (Color online) The contour plot of total energy of trigonally deformed Po calculated within the LDA without inclusion of the SO interaction. The sc structure is marked by a diamond (◇), the fcc by a triangle (△), bcc by an inverse triangle (▽), and the local minimum close to the bcc structure by a full circle. For the purpose of identification of the stationary points, the energy contours are not equidistant. The crosses (×) correspond to the uniaxial tensile test along the [111] direction; a larger asterisk marks the inflection point indicating the configuration with the maximum tensile stress.

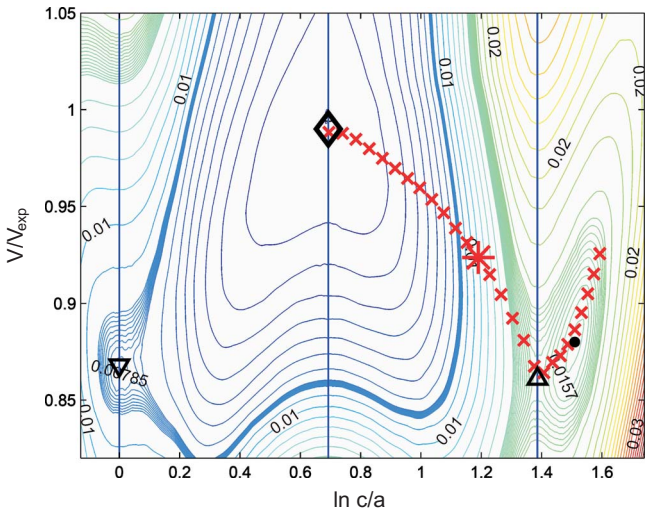

FIG. 20. (Color online) The contour plot of total energy of trigonally deformed Po calculated within the LDA and with SO interaction included. The sc structure is marked by a diamond (◇), the fcc by a triangle (△), bcc by an inverse triangle (▽), and the local minimum close to the fcc structure by a full circle. For the purpose of identification of the stationary points, the energy contours are not equidistant. The crosses (×) correspond to the uniaxial tensile test along the [111] direction; a larger asterisk marks the inflection point indicating the configuration with the maximum tensile stress.

saddle point whereas the structure belonging to the minimum close to fcc structure has a considerably larger volume than the fcc structure at the saddle point. When the SO coupling is omitted in the GGA calculations, we observe a shift of all stationary points to lower volumes and, in addition to that, both structures corresponding to the outer minima not dictated by symmetry have nearly the same atomic volume, similar to the volumes of the bcc and fcc structures at the saddle points (see also Tables II and V).

The situation is slightly changed in the LDA and LDA+SO contour plots. In the LDA contour plot (Fig. 19), the sc Po again corresponds to the absolute energy minimum (ground state) and the bcc structure at a saddle point is accompanied by a very shallow minimum at the left-hand side (at negative ln c/a). However, the fcc structure might correspond to a stationary point with a zero derivative with respect to c/a or to a saddle point followed by a very little drop of the total energy, exhibiting a very shallow, nearly unrecognizable minimum (within our convergence criterion of 0.006 mRy/atom).

When the SO interaction is included (Fig. 20), we observe again a shift of the positions of the stationary points toward higher volumes. However, now we have a stationary point with a zero derivative with respect to c/a or a saddle point followed by a very little drop of the total energy at the bcc side and a shallow minimum, not dictated by symmetry, at the fcc side. For a detailed analysis of the stationary points close to the fcc and bcc structures, we have plotted a part of the energy profiles running throughout those points in Figs. 21 and 22.

Let us note a different behavior of the total energy within the LDA and GGA and with and without inclusion of the SO coupling. One can see that the local minima are very well

TABLE V. The positions and energy differences at the local energy minima not dictated by symmetry close to the bcc (LM^{bcc}) and fcc (LM^{fcc}) structures (energies in mRy/atom) with respect to the total energy of the absolute minimum of the Po sc structure (ΔE_{sc}), or with respect to the close relevant structure at saddle point, i.e., bcc or fcc (ΔE_{loc}).

	GGA				GGA+SO			
	V/V_{exp}	ln c/a	ΔE_{sc}	ΔE_{loc}	V/V_{exp}	ln c/a	ΔE_{sc}	ΔE_{loc}
LM^{bcc}	0.88	−0.03	18.35	−0.05	0.95	−0.05	11.54	−0.06
LM^{fcc}	0.88	1.47	24.62	−0.005	1.00	1.61	18.05	−2.08
	LDA				LDA+SO			
	V/V_{exp}	ln c/a	ΔE_{sc}	ΔE_{loc}	V/V_{exp}	ln c/a	ΔE_{sc}	ΔE_{loc}
LM^{bcc}	0.82	−0.02	14.48	−0.02				
LM^{fcc}					0.87	1.50	15.54	−0.31

pronounced only close to the fcc structure in calculations with the SO coupling incorporated. The total energy corresponding to the minimum close to the equilibrium of the fcc structure in case of LDA+SO (GGA+SO) is about 0.3 (2.1) mRy/atom lower than the energy of the fcc structure. The energy differences between the local minima not dictated by symmetry and the maxima corresponding to the fcc structure at the same volume may be seen in Fig. 21 where the energy profiles along the volume-conserving trigonal deformation path are presented; the volumes, for which the profiles in Fig. 21 were calculated, are the equilibrium volumes at these local minima obtained within each approximation. Let us note that the total-energy differences obtained from this figure are slightly different from the differences ΔE_{loc} given in Table V which were calculated from energies at energy extrema. The values missing in Table V reflect the fact that no local minima were found in some cases (e.g., LDA or LDA+SO). For GGA calculation, the total-energy difference between the fcc structure and the structure at the neighboring minimum is just within our convergence criterion. In the LDA, the local minimum of total energy located behind the fcc structure is even undetectable. This suggests that, in these cases, the fcc structure may also correspond to an inflection point with respect to the c/a variable.

The total-energy profiles within the GGA and LDA without the SO coupling describing the trigonal deformation around the bcc structure (Fig. 22) are very similar in shape and energy to each other. The total-energy difference (0.05 mRy/atom) between the bcc structure and a very shallow neighboring local minimum calculated within the GGA is not affected by the SO coupling too much. The same energy difference in the case of LDA is less than half of the GGA value. Within the LDA+SO, we were not able to find any minimum close to the bcc structure and, therefore, the bcc structure may also correspond to an inflection point with respect to the c/a variable, similarly as the fcc structure for the LDA and GGA cases.

The most important conclusion of this section is that the total-energy profiles at constant volume have a very typical feature. As it can be seen from Figs. 18–20 and also from Fig. 1 from Ref. 10, all profiles, regardless of the effect of SO coupling or approximation of exchange-correlation term,

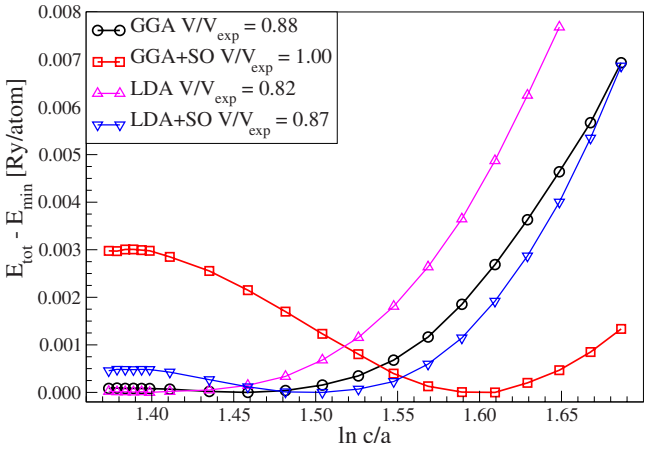

FIG. 21. (Color online) Total-energy profiles of Po along the trigonal deformation path without and with the SO interaction included in the immediate neighborhood of the fcc structure. The energy zero is given by the corresponding total-energy minima in the interval ln $c/a \in 1.37-1.68$.

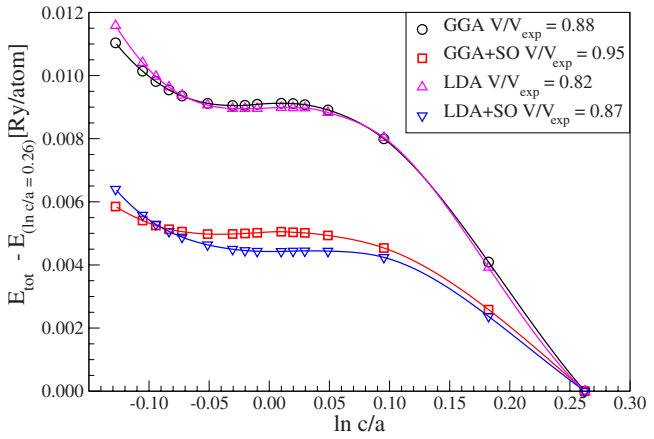

FIG. 22. (Color online) Total-energy profiles of Po along the trigonal deformation path without and with the SO interaction included in the immediate neighborhood of the bcc structure. The energy zero is given by the value of energy E_{tot} at ln $c/a=0.26$.

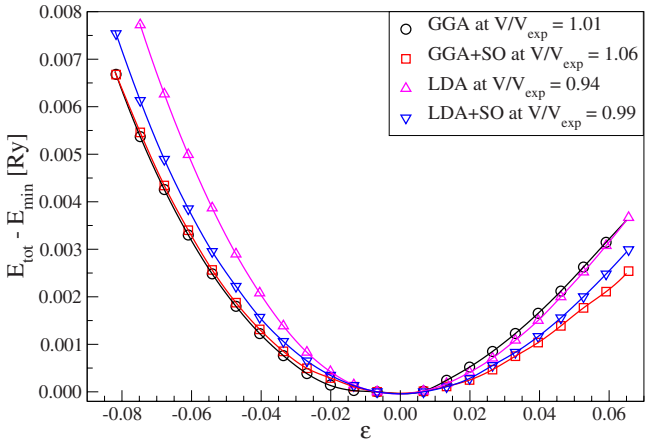

FIG. 23. (Color online) The total-energy profiles of sc Po along the tetragonal deformation path by GGA and LDA without and with the inclusion of SO coupling. The c/a ratio is recalculated to corresponding strain ε.

become flat at volumes slightly lower than the equilibrium volume and, when the volume is further decreased, they exhibit a local maximum for sc structure, accompanied by two local minima, not dictated by symmetry. As shown in Ref. 10, this means that, at slightly increased pressure, α-Po loses its cubic symmetry and a trigonal (rhombohedral) structure is preferred. We could expect a bimodal mixture of trigonal structures, one type exhibiting a value of $c/a<2$ and the other type a value of $c/a>2$ [$V/V_{\mathrm{exp}}<0.89$ (GGA and LDA) and $V/V_{\mathrm{exp}}<0.98$ (GGA and LDA with SO coupling)]. For higher volumes, the shape of the total-energy profile is roughly the same as that with the lowest total energy for the sc structure (see Fig. 17).

2. Tetragonal deformation of sc Po

The tetragonal deformation of sc Po was performed at equilibrium volumes (Table II) within LDA, LDA+SO, GGA, and GGA+SO calculations. For each curve at Fig. 23, the total energy has just one global minimum at $\varepsilon=0$ corresponding to the sc structure of Po. No other symmetry-dictated extrema exist and also no stationary point not dictated by symmetry was found in the studied range of deformations. The total energy increases on both sides of the tetragonal deformation path. The inclusion of the SO interaction decreases the curvature of the total-energy profiles (but this may also be connected with increasing atomic volume) and, therefore, decreases also the tetragonal shear modulus C'.

3. Tetragonal (Bain) path for Po

The total energy along the Bain tetragonal deformation path connecting the bcc and fcc structures (not found experimentally in Po up to now) can be displayed similarly as in the case of the trigonal path, i.e., in the form of a contour plot as a function of $\ln c/a$ and V/V_{exp}. The LDA results are presented in Fig. 24.

The GGA values exhibit a very similar picture and, therefore, they are not shown here. The total energy of the bcc

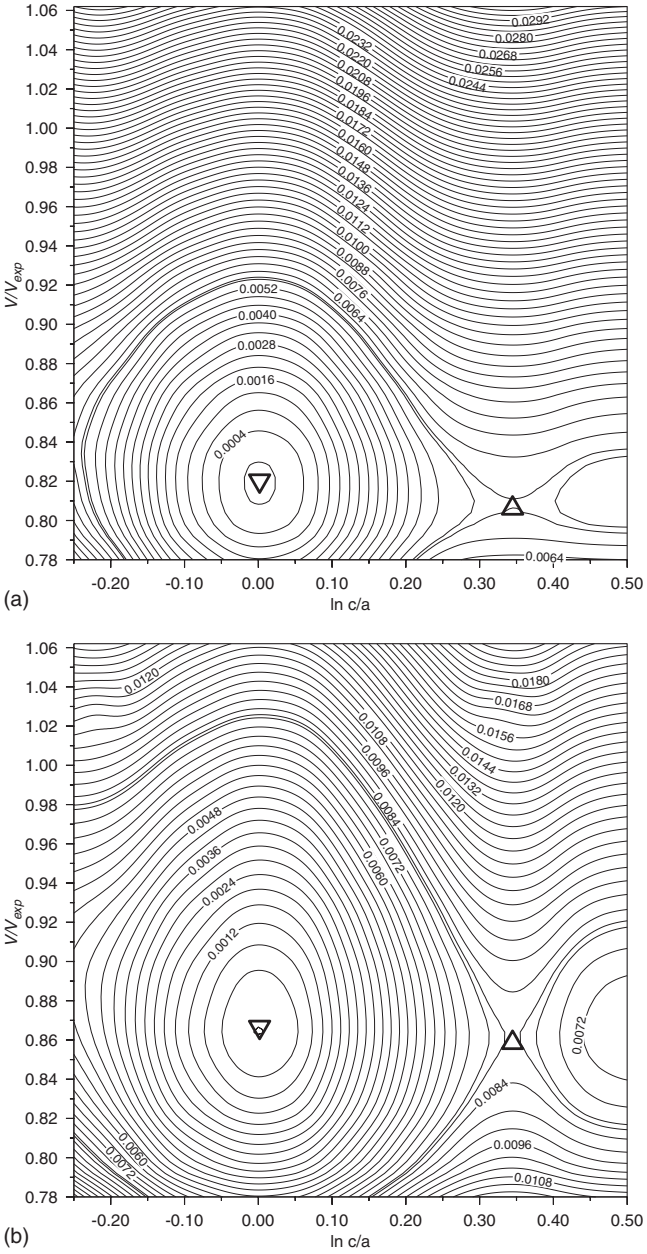

FIG. 24. The total-energy contour plots of tetragonally deformed Po calculated within the LDA without SO interaction (a) and with SO interaction included (b). The symbols ▽ and △ mark the bcc and fcc structures, respectively.

structure (marked by a ▽) is lower (see also Fig. 3) and, therefore, the total energies in the contourplots are computed with respect to the energy of the bcc structure as an energy zero. The △ indicates the total energy of the fcc structure of Po while the $\ln c/a$ ratio for the fcc structure is equal to 0.347 along the tetragonal deformation path. We have found only two symmetry-dictated stationary points: a local minimum ($E=0$) at the bcc structure and a saddle point corresponding to the fcc structure. No other extrema or stationary points of total energy are located in close vicinity of fcc and bcc structures along tetragonal deformation path. Therefore, the bcc structure of Po is stable with respect to tetragonal deformation.

TABLE VI. The tetragonal shear modulus C' (in GPa) for the hypothetical bcc and fcc structures of Po.

	LDA	GGA	LDA+SO	GGA+SO
C'_{bcc} (GPa)	10.7	13.6	15.2	14.0
C'_{fcc} (GPa)	−2.1	−3.1	−9.4	−10.8

The tetragonal shear modulus C' for hypothetical bcc and fcc structures of Po is calculated with and without the inclusion of the SO coupling (Table VI). The inclusion of SO coupling for the bcc structure calculated within the GGA does not change the C' too much whereas for the LDA, the effect of the SO interaction causes its increase by a factor of 1.5. The effect of SO coupling on the C' of the fcc structure manifests itself by an increase in $|C'|$ by a factor of 4.5 (3.5) for LDA (GGA). Let us note that the tetragonal shear moduli for the bcc structure are governed by (i.e., they are roughly proportional to) the total-energy differences between the fcc and bcc structures, in accordance with Ref. 34.

V. ELASTIC ANISOTROPY OF sc Po

More interesting than the elastic constants of hypothetical bcc and fcc structures of Po are the elastic constants of existing sc Po. Table VII summarizes our calculated values of tetragonal and trigonal shear moduli together with the values available in literature (the values of the bulk moduli B are given in Table II). Here a large elastic anisotropy of sc Po, characterized by the elastic anisotropy factor[19] $A=C_{44}/C'$, is striking.

From Table VII, one can see that the tetragonal shear modulus C' is nearly one order of magnitude higher than the trigonal shear modulus C_{44} and, therefore, the elastic anisotropy factor A is very low. In fact, the values of A are even lower when the SO coupling is taken into account and are in a strong contrast with any value of A of any single element in the periodic table. In comparison with alkali metals which exhibit the highest anisotropy factors A of all materials (7–9.4), the values for sc Po are almost two orders of magnitude lower. A slightly extended list of elastic anisotropy factors is given in Table VIII.

The elastic anisotropy of Po has already been briefly discussed in Ref. 10. Here we give some models which can further elucidate this extremely low value of the elastic anisotropy factor.

A. A pair-potential model of elastic anisotropy

Let us first employ a central-force pair-potential model (although the interatomic potential in sc Po will not be pure pair potential, we may expect that the pair-potential contribution will be dominant). Our model is based on the pair potential within the first, second, and third nearest neighbors (NN, 2NN, and 3NN, for more details see Ref. 35). Let us consider the fcc structure first. It has 12 NN at $\langle \pm 1, \pm 1, 0\rangle a/2$, $\langle \pm 1, 0, \pm 1\rangle a/2$, and $\langle 0, \pm 1, \pm 1\rangle a/2$ (a is a lattice parameter) and six 2NN at $\langle \pm 1, 0, 0\rangle a$, $\langle 0, \pm 1, 0\rangle a$, and $\langle 0, 0, \pm 1\rangle a$. If an interatomic potential $\phi(r)$ is purely radial, independent of angle, and $U=\frac{1}{2V}\Sigma\phi(r)$ is the energy density of the crystal, then the four-rank tensors for elastic moduli are given by[35,36]

$$C_{ijkl} = \frac{\delta^2 U}{\delta\varepsilon_{ij}\delta\varepsilon_{kl}} = \frac{1}{2V}[\Sigma D^2\phi(r) r_i^0 r_j^0 r_k^0 r_l^0]_{\mathbf{r}=\mathbf{r}^0}, \tag{1}$$

where the $D\phi(r)$ denotes $(1/r)[d\phi(r)/dr]$. Using Eq. (1), one obtains for the fcc structure

$$C_{1111} = C_{11} = \frac{1}{2V}\left[8\left(\frac{a}{2}\right)^4 D^2\phi\left(\frac{a}{\sqrt{2}}\right) + 2a^4 D^2\phi(a) + \cdots\right] \tag{2}$$

and

$$C_{1122} = C_{12} = C_{44} = \frac{1}{2V}\left[4\left(\frac{a}{2}\right)^4 D^2\phi\left(\frac{a}{\sqrt{2}}\right) + 0 + \cdots\right]. \tag{3}$$

The bcc structure has 8 NN at $\langle \pm 1, \pm 1, \pm 1\rangle a/2$, 6 2NN at $\langle \pm 1, 0, 0\rangle a$, $\langle 0, \pm 1, 0\rangle a$, and $\langle 0, 0, \pm 1\rangle a$ and 12 3NN at $\langle \pm 1, \pm 1, 0\rangle a$, $\langle \pm 1, 0, \pm 1\rangle a$ and $\langle 0, \pm 1, \pm 1\rangle a$. Using Eq. (1), one obtains

$$C_{11} = \frac{1}{2V}\left[8\left(\frac{a}{2}\right)^4 D^2\phi\left(\frac{\sqrt{3}a}{2}\right) + 2a^4 D^2\phi(a) + 8a^4 D^2\phi(\sqrt{2}a) + \cdots\right] \tag{4}$$

and

TABLE VII. The shear moduli C' and C_{44} (in GPa) and the elastic anisotropy factors A for sc Po obtained from the total energy in immediate neighborhood of the ground state at corresponding equilibrium volumes for both approximations for the exchange-correlation energy and with and without the effect of SO coupling. The pseudopotential calculation of Ref. 14 gives $C'=42.5$ GPa.

	LDA	GGA	LDA+SO	GGA+SO	TB (Ref. 15)	TB+SO (Ref. 15)	LDA (Ref. 15)
C'	48.3	36.6	34.4	26.8	59	52.5	36
C_{44}	3.47	3.54	2.17	4.55	2	2	5
A	0.072	0.097	0.063	0.170	0.034	0.038	0.139

TABLE VIII. The experimental values of elastic anisotropy factor $A=C_{44}/C'$ for selected elements and compounds (Ref. 4) in comparison with the present results calculated for α-Po.

Material	C' (GPa)	C_{44} (GPa)	A	T (K)	Structure
Li	1.030	8.78	8.524	298	bcc
Rb	0.230	1.71	7.435	170	bcc
Pb	4.990	19.42	3.892	273	fcc
Cu	23.100	75.70	3.277	298	fcc
Ag	15.160	46.12	3.042	300	fcc
Ni	46.600	124.20	2.665	298	fcc
Ge	40.060	66.66	1.664	298	diamond
Si	50.920	79.62	1.564	298	diamond
Al	23.170	28.34	1.223	298	fcc
W	159.010	160.83	1.011	297	bcc
V	54.850	43.20	0.788	300	bcc
NaCl	18.295	12.87	0.703	298	rocksalt
NaBr	14.845	9.98	0.672	300	rocksalt
CsCl	13.810	8.04	0.582	298	B2
Nb	56.000	28.73	0.513	300	bcc
KI	11.300	3.64	0.322	300	rocksalt
RbBr	13.260	3.80	0.287	300	rocksalt
PbTe	50.155	13.43	0.268	303	rocksalt
RbI	10.870	2.78	0.256	300	rocksalt
SnTe	52.500	11.72	0.223	300	rocksalt
α-Po(LDA)	48.3	3.47	0.072	0	sc
α-Po(GGA)	36.6	3.54	0.097	0	sc
α-Po(LDA+SO)	34.4	2.17	0.063	0	sc
α-Po(GGA+SO)	26.8	4.55	0.170	0	sc

$$C_{12}=C_{44}=\frac{1}{2V}\left[8\left(\frac{a}{2}\right)^4 D^2\phi\left(\frac{\sqrt{3}a}{2}\right)+0+4a^4D^2\phi(\sqrt{2}a)+\cdots\right]. \tag{5}$$

Finally, the sc structure has 6 NN at $\langle\pm1,0,0\rangle a$, $\langle0,\pm1,0\rangle a$, and $\langle0,0,\pm1\rangle a$, 12 2NN at $\langle\pm1,\pm1,0\rangle a$, $\langle\pm1,0,\pm1\rangle a$, and $\langle0,\pm1,\pm1\rangle a$ and 8 3NN at $\langle\pm1,\pm1,\pm1\rangle a$. Equation (1) yields

$$C_{11}=\frac{1}{2V}[2a^4D^2\phi(a)+8a^4D^2\phi(\sqrt{2}a)+\cdots] \tag{6}$$

and

$$C_{12}=C_{44}=\frac{1}{2V}[0+4a^4D^2\phi(\sqrt{2}a)+\cdots], \tag{7}$$

where 0 in Eq. (7) stands for a zero contribution of the first neighbors. The dots in the formulas indicate contributions from farther neighbors than 2NN (fcc, sc) and 3NN (bcc) which are neglected in our model. In this way, a contribution of individual coordination spheres to the elastic anisotropy factor and to the ratios of the elastic constants in fcc, bcc, and sc structures may be determined (Table IX).

It is known that the most fcc metals exhibit the values of A close to 2. This corresponds to the fact that the contribution of the first neighbors is equal to 2 and that of the second neighbors is equal to zero. On the other hand, the values of A

TABLE IX. The contributions of individual coordination spheres to the elastic anisotropy factor A and to the ratios of the elastic constants in fcc, bcc, and sc structures together with the values for Po.

	fcc		bcc			sc		
	NN	2NN	NN	2NN	3NN	NN	2NN	Po-LDA+SO
A	2	0	∞	0	2	0	2	0.063
C_{11}/C_{44}	2	∞	1	∞	2	∞	2	40.63
C_{12}/C_{44}	1	1	1	1	1	1	1	8.92

for the bcc metals range from 0.5 to 8.5 (see Table VIII) which reflects a high contribution from the NN. Surprisingly, in the sc structure, the NN do not contribute to elastic constant $C_{12}=C_{44}$ at all, therefore we can expect a relation $C_{12} \ll C_{11}$. In reality, there are also nonpair and noncentral contributions in interatomic interactions and, therefore, the value of C_{44} somewhat differs from the value of C_{12}; the Cauchy relation $C_{12}=C_{44}$ for the cubic structure does not hold in real Po. The trigonal shear modulus C_{44} of Po is even several times smaller than C_{12}. The value of tetragonal shear modulus is dominated by C_{11} and, according to Table IX, it may be much larger than C_{44} which may be expected to be very low. This corresponds to a small value of the elastic anisotropy factor A, where the contribution of the first neighbors is completely missing. The second neighbors in the simple cubic and in the NaCl structures are $\sqrt{2}$ times farther and their contribution to the values of A will be also much smaller (the weight of $A=2$ in Table IX will be much lower).

B. A potential-independent model

In an open structure such as sc or NaCl structure, we may suppose that for elastic constants, the behavior of the first coordination shell will be dominant. Now, let us apply the same uniaxial deformation along the [001] and [111] axes, i.e., the tetragonal and trigonal deformation, respectively. In the coordination system where the loading axis is the z axis, the corresponding deformation tensor is $\varepsilon=\mathrm{diag}(-\frac{\varepsilon}{2},-\frac{\varepsilon}{2},\varepsilon)$, where ε is the relative elongation along the loading axis. The deformation energy per unit of volume is $\frac{3}{2}C'\varepsilon^2$ and $\frac{3}{2}C_{44}\varepsilon^2$ for tetragonal and trigonal deformation, respectively. In the sc or NaCl structure, the first coordination sphere consists of six atoms at $\pm\langle 1,0,0\rangle$, $\pm\langle 0,1,0\rangle$, and $\pm\langle 0,0,1\rangle$ positions. When we perform the tetragonal deformation, four nearest-neighbor bonds are shortened by $-\frac{\varepsilon}{2}$ and two of them are elongated by ε. In the case of trigonal deformation, all bonds are elongated by $\frac{\varepsilon^2}{2}$. If no very strong angular forces are present (which may be supposed in an *sp* metal or in ionic materials with the NaCl structure), then the elastic energy is proportional to the squares of the changes in the lengths of bonds. For tetragonal deformation, the changes in the lengths of bonds provide a deformation energy proportional to ε^2 but in the case of trigonal deformation, the corresponding deformation energy is of the order of ε^4, the quadratic term is completely missing and, therefore, at least in this approximation, the C_{44} is zero. A small positive value of C_{44} in these solids is then due to the effect of the second neighbors and/or weak angular forces which deliver a small contribution to the deformation energy proportional to ε^2.

Therefore, extremely low values of the elastic anisotropy factor in sc Po and in compounds with the NaCl lattice are intimately connected with their crystal structure. Comparing the values of A for sc Po, regardless of approximations used, with the materials at the end of the Table VIII, those having $A<0.4$ all belong to the ionic NaCl prototype structure. If the atoms of the AB rocksalt structure would be just of one kind then the result is the sc structure. There is another common feature between the sc Po and rocksalt structures materials with very low elastic anisotropy ($A<0.4$), such as KBr, KI, RbI, and RbCl. Both can suppress the Peierls distortion. When the electronegativity between A and B is very high the energy degeneracies at cation and anion (A,B) differ remarkably for this highly ionic situation and then the Peierls distortion is switched off.[37]

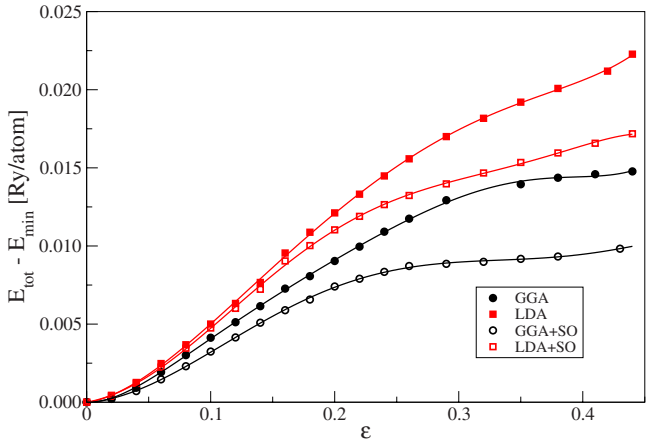

FIG. 25. (Color online) The total energy (in Ry/atom) as a function of elongation ε of sc Po along the [001] loading direction using LDA and GGA with and without SO coupling. The data points are fitted by a sixth-order polynomial.

VI. IDEAL STRENGTH AND DUCTILITY OF PO

Next mechanical property of interest, after elastic constants, is theoretical tensile strength which constitutes the upper limit of stresses which can be accommodated by a defect-free material (see Refs. 6, 38, and 39, and references therein). This information may be particularly valuable for Po which is highly radioactive and, presumably, no tensile tests will be performed experimentally in near future.

We have simulated uniaxial tensile tests for deformations along the [001] and [111] directions as described, e.g., in Refs. 38–40. In Figs. 25 and 26, we display the total energy

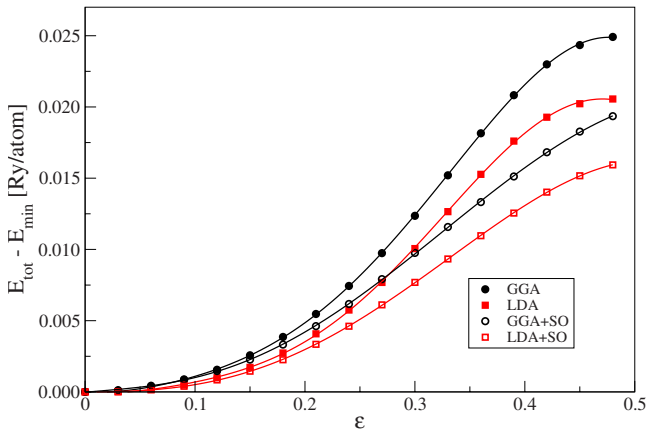

FIG. 26. (Color online) The total energy (in Ry/atom) as a function of elongation ε of sc Po along the [111] loading direction using LDA and GGA with and without SO interaction. The data points are fitted by a sixth-order polynomial.

TABLE X. The ideal tensile strengths σ^{th} (in GPa) for the tensile loading along the [001] ($\sigma^{\mathrm{th}}_{[001]}$) and [111] directions ($\sigma^{\mathrm{th}}_{[111]}$) together with the elongations $\varepsilon^{\mathrm{th}}_{[001]}$ and $\varepsilon^{\mathrm{th}}_{[111]}$ that correspond to the states in which the theoretical tensile strengths are achieved. The error bar of the positions of the inflection points may be estimated as ± 0.02 and that of the theoretical tensile strengths as about ± 0.2 GPa.

Method	$\sigma^{\mathrm{th}}_{[001]}$	$\varepsilon^{\mathrm{th}}_{[001]}$	$\sigma^{\mathrm{th}}_{[111]}$	$\varepsilon^{\mathrm{th}}_{[111]}$
LDA	4.7	0.13	7.6	0.34
GGA	3.3	0.12	7.8	0.34
LDA+SO	4.2	0.10	4.7	0.33
GGA+SO	2.6	0.10	4.7	0.33

of Po as a function of loading along the [001] and [111] directions calculated within both approximations for the exchange-correlation energy, LDA and GGA, and including or omitting the SO coupling. We are mainly interested in the first inflection point at the total-energy profile when material is loaded. This point determines the maximum stress the crystal can sustain provided that some other instabilities (soft phonons, violation of some other stability condition, etc.) do not occur prior to reaching the inflection point; in those cases, the stress corresponding to these instabilities would determine the theoretical strength for a given mode of loading. The calculated theoretical strengths of Po are summarized in Table X together with corresponding elongations. In general, total-energy profiles for the tensile test along the [001] direction calculated within the GGA and GGA+SO lie below those obtained within the LDA and LDA+SO, respectively. This is also reflected in the corresponding values of theoretical strength $\sigma^{\mathrm{th}}_{[001]}$, which range between 2.6 and 4.7 GPa. In the tensile test along the [111] direction, the situation is nearly opposite. The total-energy profile for GGA is above that for LDA and that one for GGA+SO lies above that for LDA+SO in the region around and above the inflection point. Again, this ordering may also be seen in the ordering of theoretical strengths $\sigma^{\mathrm{th}}_{[111]}$ along the [111] direction, which range from 4.7 to 7.8 GPa. Let us note that the slopes of the curves in Figs. 25 and 26 at their inflection points do not give directly the values of theoretical strengths, as also the difference in atomic volumes in each case must be considered. That is why the theoretical strengths from the LDA and GGA as well as for the LDA+SO and GGA+SO profiles for loading along the [111] direction are nearly the same, although the slopes of the profiles are different. Interestingly enough, in the LDA+SO approach which we consider as most reliable here, the theoretical strengths for the [001] and [111] loading are nearly equal ($\sigma^{\mathrm{th}}_{[111]}/\sigma^{\mathrm{th}}_{[001]}=1.12$). Therefore, polonium, which is strongly elastically anisotropic at small deformations, exhibits nearly isotropic theoretical strengths. On the other hand, tungsten, which is nearly elastically isotropic at small deformations ($A \approx 1$), has quite anisotropic theoretical strengths ($\sigma^{\mathrm{th}}_{[111]}/\sigma^{\mathrm{th}}_{[001]}=1.39$, Ref. 40).

Figures 18–20 show the paths corresponding to the uniaxial tensile tests along the [111] direction calculated within the GGA+SO, LDA, and LDA+SO, marked by crosses ($\times$). Clearly, each path starts at the absolute minimum corresponding to the sc structure ($\diamond$), continues towards the saddle point (fcc structure denoted by a $\triangle$) and, in cases of GGA, GGA+SO, and LDA+SO calculations, into the local minimum at $\ln c/a > 1.4$, keeping the lowest total-energy gradient. The asterisk ($*$) marks the inflection point of the total energy along this path. Of course, the stability limit (theoretical strength) is reached far before arriving at the fcc saddle point, at $\varepsilon^{\mathrm{th}}_{[111]}=0.33-0.34$ whereas the fcc structure corresponds to $\varepsilon_{[111]}=0.587$. Only the path up to the strength limit is relevant; after that the deformed structure looses its stability.

In general, the ideal tensile strength along the [111] direction is higher than along [001] (Table X). The inclusion of the SO coupling lowers the values of tensile strength, regardless the direction of loading. However, the significant difference between tensile tests along [001] and [111] loadings is the elongation corresponding to the tensile strength. Along the [111] direction, the elongations are about three times higher than those along the [001]. This can be explained by the low values of the trigonal shear modulus C_{44}. For trigonal deformation the material resistance is very weak, and even weaker when the SO interaction is included. This is connected with the fact that in the sc structure, the cubic unit cell is empty at the center and it is relatively easy to deform it uniaxially along the body diagonal. The total energy increase along the tetragonal deformation in the neighborhood of the sc Po is much higher than in the case of trigonal deformation.

An interesting feature of tensile tests for the [111] loading is the behavior of the atomic volume (see the crosses in Figs. 18–20). In the neighborhood of the sc structure, it is closely connected with the value of the Poisson ratio for uniaxial loading along this direction $\nu[111]=(C_{11}+2C_{12}-2C_{44})/(2C_{11}+4C_{12}+2C_{44})=0.475$ (LDA+SO calculation), which is not very different from the value of 0.5 corresponding to incompressible material. This is reflected in a nearly constant value of the atomic volume around the sc structure. After a very small increase with the gradient of $(\Delta V/V)/\varepsilon = 1-2\nu[111]$, barely seen in Figs. 18–20, the atomic volume strongly decreases towards the value for the fcc structure (by about 7% in Fig. 20 when reaching the inflection point). This behavior is due to the fact that the fcc structure (which, as a higher-symmetry structure, also lies on the uniaxial deformation path for the tensile test and is reached for positive tensile strains) exhibits considerably lower equilibrium volume than the sc structure.

A decreasing volume for positive tensile strains is in contrast to the behavior reported for other systems studied in our group, as, e.g., $MoSi_2$ or Fe (see, e.g., Refs. 41–43), where the volume increases nearly linearly up to the inflection point. This is also the case of the tensile test of tetragonally deformed sc Po, where $\nu[001]=0.180$ (LDA+SO) and, therefore, the volume is increased during tetragonal tension.

Of course, we may analyze the behavior of Poisson ratio for all uniaxial deformations.[44] It turns out that the extreme values of Poisson ratio for sc Po are $\nu[110,001]=0.018$ and $\nu[110,1\bar{1}0]=0.916$ for uniaxial deformation along the [110] direction and contractions along the directions [001] and

$[1\bar{1}0]$, respectively. Therefore, sc Po is not an auxetic material and its Poisson ratio is never negative, in contrast, e.g., to some orientations in Cu, Pb, Ca, Na, and Li (Ref. 45) where negative values were reported. Further, the Poisson ratio of sc Po for uniaxial deformation along the [110] direction averaged with respect to transverse directions[46] is 0.467, not very different from the value of $\nu[111]$.

Thus, uniaxial deformation of sc Po is strongly anisotropic. For a tensile test along the [001] direction, we have an isotropic contraction in the (001) plane with a strongly increasing volume $[\nu[001]=0.180, (\Delta V/V)/\varepsilon=1-2\nu[001]=0.64]$, for a tension along the [111] direction, we observe also an isotropic contraction in the (111) plane but the volume is nearly constant $[\nu[111]=0.475, (\Delta V/V)/\varepsilon=1-2\nu[111]=0.05]$, and for a tension along the [110] direction, we encounter nearly no contraction along the [001] direction $(\nu[110,001]=0.018)$ but a very strong contraction along the $[1\bar{1}0]$ direction $(\nu[110,1\bar{1}0]=0.916)$ and, again, the atomic volume during the deformation is nearly constant.

On the basis of the of the calculated elastic constants, we can also predict whether sc Po will be brittle or ductile. The isotropic shear modulus in the Voigt and Reuss approximations amounts to $G_V=15.1$ GPa and $G_R=3.5$ GPa, respectively, the arithmetic average is $G_A=9.3$ GPa (here and henceforth, we use again the elastic constants calculated within the LDA+SO). The corresponding values of B/G are 2.8, 12.1, and 4.6, respectively, which means, according to Pugh criterion,[47] that Po should be ductile ($B/G>1.75$ for ductile materials). Another criterion for ductility is the effective polycrystalline Poisson ratio $\nu=(3B-2G)/(6B+2G)$, which amounts to 0.34 and 0.46 for Voigt and Reuss approximation of G and 0.40 for averaged G_A. According to Frantsevich,[48] if $\nu>1/3$, the material may be expected to be ductile. This condition is met by all three values of ν calculated.

Finally, let us also mention the Cauchy pressure $C_{12}-C_{44}$. It reflects the angular character of atomic bonding in solids[49] which also relates to brittle or ductile behavior. If it is positive, the bonding is metallic but it is negative for directional bonding with angular (covalent) character. In our case, $C_{12}-C_{44}=17.2$ GPa. This is a strongly positive value and, therefore, we can expect metallic bonding, which is also in agreement with metallic density of states [see Fig. 4(a)].

Thus, on the basis of the above considerations, we predict that sc α-Po is a ductile material. Hopefully, this prediction can be verified experimentally in foreseeable future.

VII. CONCLUSIONS

Using the state-of-the-art *ab initio* electronic-structure calculations, we analyzed and explained the stability of simple cubic structure of α-Po, elucidated its extreme elastic anisotropy and calculated its theoretical tensile strength for uniaxial loading along the [001] and [111] directions. It turns out that there are two possible agents stabilizing the simple cubic structure of Po: relativistic effects of core electrons, as found in this work, or spin-orbit interaction of $6p$ electrons.[18] Here we can see a delicate interplay of individual terms in total energy determining finally that simple cubic structure of Po is energetically more favorable than trigonal spiral structure of Te and Se, which are in the same column of the periodic table. Application of a modest pressure destabilizes the simple cubic structure in Po—we may expect a bimodal mixture of trigonal structures. Extreme elastic anisotropy of α-Po is a direct consequence of its simple cubic structure and, roughly speaking, may be understood on the basis of the fact that the unit cell of the simple cubic structure is empty in the middle so that uniaxial deformation along the body diagonal is much easier than along the cube edge. Also Poisson ratio exhibits a strong anisotropy. Its value for the [110] direction averaged with respect to transverse directions and the value for the [111] direction are not very far from 0.5, which corresponds to an incompressible solid, but for the [001] direction, we have a value about 2.5 times lower. This is also reflected in behavior of α-Po during the tensile tests along the [111] and [001] directions. The values of Poisson ratio for all directions are positive, so that α-Po is not auxetic. Finally, Po is quite a soft material. Its theoretical tensile strengths amount to 4.2 GPa and 4.7 GPa for the loading along the [001] and [111] directions, respectively, so that it is much weaker than most of metals studied up to now (for a review see, e.g., Refs. 6, 38, and 39). On the basis of Pugh and Frantsevich criteria, we predict that α-Po is ductile. A positive value of the Cauchy pressure confirms the metallic type of bonding. As there is not too much experimental information on Po, most of our results are theoretical predictions. We hope that they may motivate experimentalists to confirm or disprove at least some of them.

ACKNOWLEDGMENTS

Fruitful discussions with Jan Kuneš and Pavel Novák as well as their substantial help in the early stages of our calculations are gratefully acknowledged. This research was supported by the Grant Agency of the Czech Republic (Projects No. 202/06/1509 and No. 202/09/1786), by the Grant Agency of the Academy of Sciences of the Czech Republic (Project No. IAA100100920), and by the Research Project No. AV0Z20410507 of the Academy of Sciences of the Czech Republic and Project No. MSM0021622410 of the Ministry of Education of the Czech Republic.

*legut@ipm.cz

[1] W. H. Beamer and C. R. Maxwell, J. Chem. Phys. **14**, 569 (1946).
[2] W. H. Beamer and C. R. Maxwell, J. Chem. Phys. **17**, 1293 (1949).
[3] J. M. Goode, J. Chem. Phys. **26**, 1269 (1957).
[4] *Handbook of Chemistry and Physics*, 57th ed. (CRC Press, Cleveland, OH, 1976).
[5] A. E. Mattsson, P. A. Schultz, M. P. Desjarlais, T. R. Mattsson, and K. Leung, Modell. Simul. Mater. Sci. Eng. **13**, R1 (2005).
[6] S. Ogata, Y. Umeno, and M. Kohyama, Modell. Simul. Mater. Sci. Eng. **17**, 013001 (2009).
[7] L. Lohr, Inorg. Chem. **26**, 2005 (1987).
[8] D. Legut, M.S. thesis, Brno University of Technology, 2000.
[9] D. Legut, Ph.D. thesis, Brno University of Technology, 2004.
[10] D. Legut, M. Friák, and M. Šob, Phys. Rev. Lett. **99**, 016402 (2007).
[11] D. Legut, Phys. Today **60**(10), 17 (2007).
[12] D. Legut, M. Friák, and M. Šob, Phys. Today **61**(9), 10 (2008).
[13] M. Šob, D. Legut, and M. Friák, Phys. Rev. Lett. **102**, 079702 (2009).
[14] R. E. Kraig, D. Roundy, and M. L. Cohen, Solid State Commun. **129**, 411 (2004).
[15] M. Lach-hab, B. Akdim, D. A. Papaconstantopoulos, M. J. Mehl, and N. Bernstein, J. Phys. Chem. Solids **65**, 1837 (2004).
[16] B. I. Min, J. H. Shim, M. S. Park, K. Kim, S. K. Kwon, and S. J. Youn, Phys. Rev. B **73**, 132102 (2006).
[17] N. A. Zabidi, H. A. Kassim, and K. N. Shristava, *Current Issues of Physics in Malaysia: National Physics Conference 2007*, PERFIK 2007, AIP Conf. Proc. No. 1017 (AIP, New York, 2008), p. 255.
[18] K. Kim, H. C. Choi, and B. I. Min, Phys. Rev. Lett. **102**, 079701 (2009).
[19] C. Zener, *Elasticity and Anelasticity of Metals* (University of Chicago Press, Chicago, IL, 1948).
[20] P. Blaha, K. Schwarz, G. K. H. Madsen, D. Kvasnicka, and J. Luitz, *An Augmented Plane Wave Plus Local Orbitals Program for Calculating Crystal Properties* (Technical University Vienna, Vienna, Austria 2001).
[21] J. P. Perdew and Y. Wang, Phys. Rev. B **45**, 13244 (1992).
[22] J. P. Perdew, K. Burke, and M. Ernzerhof, Phys. Rev. Lett. **77**, 3865 (1996).
[23] M. Šob, L. G. Wang, and V. Vitek, Comput. Mater. Sci. **8**, 100 (1997).
[24] P. J. Craievich, M. Weinert, J. M. Sanchez, and R. E. Watson, Phys. Rev. Lett. **72**, 3076 (1994).
[25] D. Legut and M. Šob, Mater. Sci. Forum **567-568**, 77 (2008).
[26] J. Stöhr and H. C. Siegmann, *Magnetism From Fundamentals to Nanoscale Dynamics* (Springer, Berlin, New York, 2006).
[27] K. G. Dyall, P. R. Taylor, K. Faegri, and L. Partridge, J. Chem. Phys. **95**, 2583 (1991).
[28] N. V. Sidgwick, *Some Physical Properties of the Covalent Link in Chemistry* (Cornell University Press, Ithaca, NY, 1933), Vol. 210, p. 189.
[29] A. von Hippel, J. Chem. Phys. **16**, 372 (1948).
[30] R. Keller, W. B. Holzapfel, and H. Schulz, Phys. Rev. B **16**, 4404 (1977).
[31] M. I. McMahon and R. J. Nelmes, Chem. Soc. Rev. **35**, 943 (2006).
[32] M. J. Verstraete, Phys. Rev. Lett. **104**, 035501 (2010).
[33] D. Legut, M. Friák, and M. Šob, in Proceedings of International Conference Juniormat'01, edited by J. Švejcar (Brno University of Technology, Brno, 2001) p. 198.
[34] P. Söderlind, O. Eriksson, J. M. Wills, and A. M. Boring, Phys. Rev. B **48**, 5844 (1993).
[35] H. M. Ledbetter and R. L. Moment, Acta Metall. **24**, 891 (1976).
[36] E. R. Fuller, A. V. Granato, J. Holder, and E. R. Naimon, *Methods of Experimental Physics* (Academic Press, New York, 1974), Vol. 11.
[37] J. K. Burdett, *Chemical Bonding in Solids* (Oxford University Press, New York, 1995).
[38] M. Šob, M. Friák, D. Legut, J. Fiala, and V. Vitek, Mater. Sci. Eng., A **387-389**, 148 (2004).
[39] J. Pokluda, M. Černý, P. Šandera, and M. Šob, J. Comput.-Aided Mater. Des. **11**, 1 (2004).
[40] M. Šob, L. G. Wang, and V. Vitek, Mater. Sci. Eng., A **234-236**, 1075 (1997).
[41] M. Friák, M. Šob, and V. Vitek, Phys. Rev. B **68**, 184101 (2003).
[42] M. Friák, M. Šob, and V. Vitek, Philos. Mag. **83**, 3529 (2003).
[43] M. Šob and M. Friák, Intermetallics **17**, 523 (2009).
[44] A. N. Norris, Proc. R. Soc. London, Ser. A **462**, 3385 (2006).
[45] R. V. Goldstein, V. A. Gorotsov, and D. S. Lisovenko, Dokl. Phys. **54**, 546 (2009).
[46] K. W. Wojciechowski, Comput. Methods Sci. Technol. **11**, 73 (2005).
[47] S. F. Pugh, Philos. Mag. **45**, 823 (1954).
[48] I. N. Frantsevich, F. F. Voronov, and S. A. Bokuta, in *Elastic Constants and Elastic Moduli of Metals and Insulators Handbook*, edited by I. N. Frantsevich (Naukova Dumka, Kiev, 1983), p. 60.
[49] D. G. Pettifor, Mater. Sci. Technol. **8**, 345 (1992).